THE UNIVERSITY OF CHICAGO

LOCAL OPERATIONS FOR ENTANGLED STATES IN QUANTUM SYSTEMS: TRANSFER, TOMOGRAPHY, AND MANIPULATION

A DISSERTATION SUBMITTED TO
THE FACULTY OF THE PRITZKER SCHOOL OF MOLECULAR ENGINEERING
IN CANDIDACY FOR THE DEGREE OF
DOCTOR OF PHILOSOPHY

BY
YAT WONG

CHICAGO, ILLINOIS
DECEMBER 2025

ABSTRACT

In addition to the quality of the controls, one factor that is often overlooked is the spectrum of available controls. This dissertation demonstrates how small differences in local operation capabilities can affect overall performance for entanglement generation, verification, and manipulation: in a photon capture process, how access to reflection permits perfect capture in the noiseless regime and improve efficiency in the noisy regime; how Pauli measurements are not suitable for verifying some simplest possible states; and how a single qudit gate can facilitate manipulation of entanglement with local Clifford gates in tripartite stabilizer states over qudits with nonsquarefree levels.

Life is so unpredictable, but sometimes only when viewed from the surface.

One moment I was complaining about how I am basically learning nothing in my seventh grade class, and at the next moment I was discussing with my teachers about skipping two grades. Or I was repining how my courses in the first semester in the university were just repeating what I have learned in the Olympiad trainings, and before I realized I was already deregistering from the university to go to a more flexible one instead.

Back then, I never thought about how much work was done behind the scenes, or why we lived relatively well-off, and all I did was grumbling about things like how I was forced to practice for competitions instead of going out in the Lunar New Year.

Now that I have lived on my own for years and learned to appreciate, and several of my family members' health are deteriorating, yet I am stuck here due to visa shenanigans.

This is dedicated to my family, especially my parents.

I still think things like forcing practice during the holidays were cruel though.

TABLE OF CONTENTS

LIST OF FIGURES

LIST OF TABLES

ACKNOWLEDGMENTS

First and foremost, this endeavor would not have been possible without my advisor Prof. Liang Jiang and his tremendous support and guidance throughout my PhD. I am also thankful to my defense committee and candidacy committee for their precious expertise, knowledge, and insights. Additionally, thanks should also go to my collaborators, both internal and external, and friends in Jiang group and the broader Pritzker School of Molecular Engineering community.

I would also like to extend my sincere thanks to my friends and teachers that led my journey towards physics, including the mathematics and physics Olympiad community in Hong Kong; the friends and teachers from my primary and secondary school, especially my physics teacher Alex O; the friends and professors from CUHK and HKUST, especially my undergraduate academic advisor Prof. Kam Tuen Law.

Lastly, words cannot express my gratitude to my family, especially my parents Shing Hung Wong and King Hung Cheng. Despite exhausting jobs, they provided tremendous unspoken love and support that I only learned to appreciate in recent years as I started to mature.

CHAPTER 1

INTRODUCTION

Quantum information, the product of the overlapping between quantum mechanics and information theory, is signified by superposition and entanglement. The former is usually represented by the famous "Schrödinger's cat" thought experiment, while the latter is best illustrated by the EPR paradox. The EPR paradox, a thought experiment proposed by Einstein, Podolsky, and Rosen to argue that quantum mechanics, which Einstein himself contributed heavily himself, is incomplete, ironically became the hallmark of quantum entanglement. The implication of this thought experiment, coined as "spooky action in a distance" by Einstein and formalized by Bohm and Bell, is the existence of quantum states that cannot be described as a classical (correlated) mixture of uncorrelated states. Such states, now known as entangled states, underpin many applications of quantum information, including information-theoretically secure cryptography, quantum telescope, and distributed quantum computing.

The technologies arising from quantum information can roughly be divided into three major branches: quantum computation, which mainly relies on superposition to outperform classical counterparts; quantum metrology and sensing, leveraging superposition to accumulate information of the sensed parameters; and quantum communication and cryptography, where entanglement is used to transmit information in ways classically impossible. Note that these branches do not only use one aspect exclusively: to build a scalable quantum computer, individual components with entangling capabilities are required; and quantum cryptography relies on no cloning theorem, which can be viewed as an implication of superposition. Moreover, such classification is neither exhaustive nor exclusive, as there are technologies that are in crossovers of these branches, such as quantum telescope, which is a quantum sensing application that requires quantum communication between distant detectors [1]; and distributed quantum computing, which can perform multipartite computation

tasks impossible in classical systems [2].

Thus, distribution, verification, and manipulation of entangled states are crucial to many quantum technologies. Numerous schemes have been proposed to facilitate such processes, including quantum transduction, repeaters, vacuum beam guides, satellite-assisted quantum state transfer, etc. for distribution of quantum entanglement; shadow tomography, principle component analysis, matrix product state tomography, etc. for quantum state estimation. Much effort has been devoted to optimize different methods. One often underappreciated direction is how small additions to capabilities influence the efficacy of performing quantum processes. For example, it is well known that Clifford gates, generated by Hadamard gate H, phase gate S, and controlled-NOT $CNOT$, with addition of a non-Clifford gate, usually T gate, is universal, and most works have been focusing around maximizing the fidelity of Clifford gates and T gates, due to the ease of implementation for CSS codes. However, [Error-structure-tailored fault-tolerance and early fault-tolerant quantum computing] recently showed that by tailoring small angle rotations, qubit rotations of arbitrary angles and thus arbitrary gates can be performed faster with higher fidelity compared to T gate based compilation. This dissertation similarly focuses on how local capabilities affect creation, certification, and control of quantum entanglement.

1.1 Dissertation Structure and Personal Achievements

This dissertation covers the following three projects:

- Chapter 3, adapted from [3], depicts a photon capture scheme inspired by a transduction project in collaboration with Rigetti, Harvard, and MIT [4]. This scheme addresses the issue of initial reflection when capturing an incoming pulse using a cavity with finite coupling by redirecting the reflection back to the cavity after a delay. With well-adjusted coupling and delay, such scheme permits perfect capture of the incoming pulse in the noiseless regime and enhances fidelity under intrinsic losses.

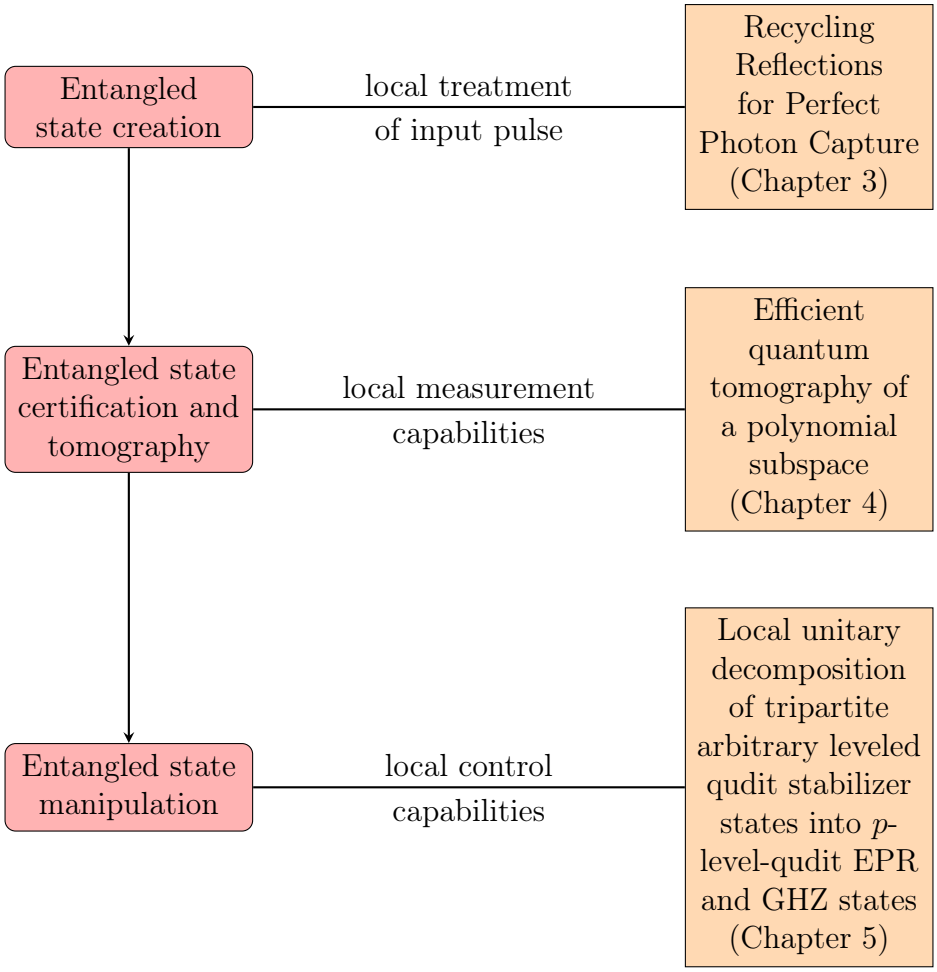

Figure 1.1: Thesis roadmap. Red blocks on the left represents stages in entangled state preparation, orange blocks on the right represents projects covered in this thesis, and the links between represents the influence of local capabilities analyzed in the projects for the corresponding stages.

- Chapter 4, adapted from [5], describes a state certification and subspace tomography scheme driven by a multimode blockade experiment [6]. Utilizing measurements beyond Pauli measurements for qubits and Wigner measurements for CV systems, this scheme reduces the state verification overhead of certain states exponentially. This method is then extended to subspace tomography, leveraging the structure of the Hilbert space of multimode systems.

- Chapter 5, adapted from [7], presents a decomposition procedure of tripartite stabilizer states of qudits with any integer levels, including powers of primes, into EPR pairs and GHZ states using only local unitaries. This fills a gap in the existing literature, as previously this was only shown for squarefree leveled qudits, and reaffirms that tripartite stabilizer states only exhibit EPR and GHZ type entanglements.

Apart from projects covered in this dissertation, I also participated in multiple other projects:

- "Entanglement-enabled advantage for learning a bosonic random displacement channel" [8, 9] led by Changhun Oh, Senrui Chen, and Zheng-Hao Liu, where I assisted in proving the sampling lower bound for sensing with unentangled inputs.

- "Peer-to-Peer Distribution of Graph States Across Spacetime Quantum Networks of Arbitrary Topology" [10] led by Yuexun Huang, where I proved an integral multisink flow can be executed as the sum of integral flows on a collection of integral flow networks with shared graph if and only if the flow is a valid flow for the flow network with each edge's capacity being the sum of the capacities in the collection.

- "Universal spreading of conditional mutual information in noisy random circuits" [11] led by Su-un Lee, where I provided insights for mechanisms of stabilizer generator length extension by noise and the implications.

- "Optimality Condition for the Petz Map" [12] led by Bikun Li, where I provided examples where I provided nontrivial examples of Petz Map being optimal when Knill-

Laflamme conditions are not satisfied and the input state does not commute with the reference state.

- “Quantum-inspired classical algorithms for molecular vibronic spectra" [13] led by Changhun Oh, where I helped to convert the algorithm from a classical stocastic algorithm to a deterministic algorithm.

- “Optimized protocols for duplex quantum transduction" [14] led by Zhaoyou Wang, where I assisted in generating the Pareto frontier of achievable rates.

- “Quantum limits of superresolution in a noisy environment" [15] led by Changhun Oh, where I participated in the calculation of the Quantum Fisher Information.

- “Path-independent quantum gates with noisy ancilla" [16] led by Wen-Long Ma, where I provided the template of using Dyson expansion as analysis for SNAP gate implementation, which was then generalized to become the basis of the paper.

CHAPTER 2

PRELIMINARIES

This chapter provides preliminaries for the projects covered in this dissertation, one section for each chapter.

2.1 Quantum Input/Output Relations

Quantum input/output relations were developed to model the time dynamics of a quantum system interacting with a thermal bath [17]. The thermal bath is modeled to interact with the system through a system operator c in the following Hamiltonian:

$$\begin{aligned} H &= H_{\text{sys}} + H_B + H_{\text{int}} \\ H_B &= \hbar \int_{-\infty}^{\infty} \omega b^\dagger(\omega) b(\omega) d\omega \\ H_{\text{int}} &= i\hbar \int_{-\infty}^{\infty} \kappa(\omega) \left(b^\dagger(\omega) c - c^\dagger b(\omega) \right) d\omega \end{aligned} \tag{2.1}$$

where $b(\omega)$ are the bath annihilation operators satisfying $[b(\omega), b^\dagger(\omega')] = \delta(\omega - \omega')$. Application of the Markov approximation in the form of $\kappa(\omega) = \sqrt{\frac{\gamma}{2\pi}}$ and Fourier transform of the bath operator $b_{\text{in}}(t) = (2\pi)^{-1/2} \int_{-\infty}^{\infty} e^{-i\omega(t-t_0)} \left[b(\omega) \right]_{t_0} d\omega$, where $t_0 < t$, results in the quantum Langevin equation of any system operator a:

$$\frac{d}{dt} a = -\frac{i}{\hbar} [a, H_{\text{sys}}] - [a, c^\dagger] \left(\frac{\gamma}{2} c + \sqrt{\gamma} b_{\text{in}}(t) \right) - \left(\frac{\gamma}{2} c^\dagger + \sqrt{\gamma} b_{\text{in}}^\dagger(t) \right) [a, c] \tag{2.2}$$

For a harmonic oscillator with $H_{\text{sys}} = \hbar\omega_0 a^\dagger a$ and $c = a$, this reduces to

$$\frac{d}{dt} a = -i\omega_0 a - \frac{\gamma}{2} a - \sqrt{\gamma} b_{\text{in}}(t) \tag{2.3}$$

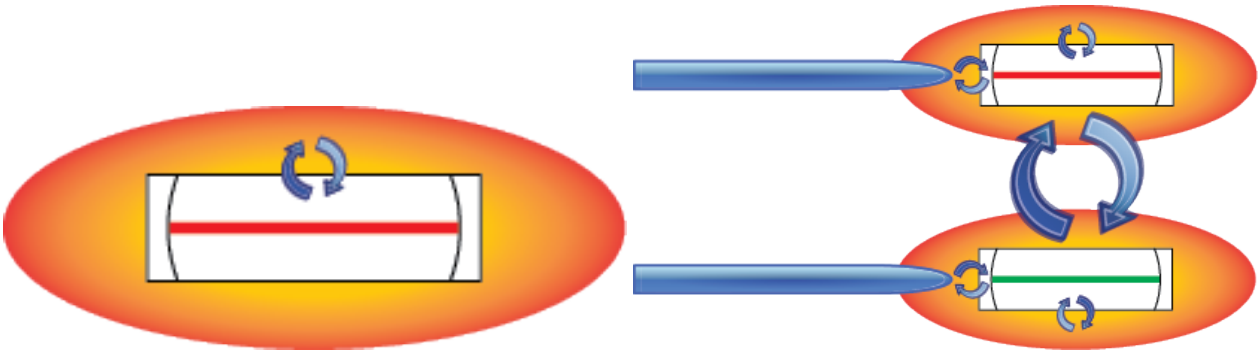

(a) (b)

Figure 2.1: Schematics of (a) a cavity interacting with a thermal bath, and (b) a transducer depicted as two interacting cavities, each interacting with their own thermal bath and external input/output.

An alternative Fourier transform of $b_{\text{out}}(t) = (2\pi)^{-1/2} \int_{-\infty}^{\infty} e^{-i\omega(t-t_1)} \left[b(\omega)\right]_{t_1} d\omega$ with $t_1 > t$ results in

$$\frac{d}{dt}a = -i\omega_0 a + \frac{\gamma}{2}a - \sqrt{\gamma}b_{\text{out}}(t) \tag{2.4}$$

and hence

$$b_{\text{out}}(t) - b_{\text{in}}(t) = \sqrt{\gamma}a(t). \tag{2.5}$$

These operators are interpreted as the input from the bath to the system and the output from the system to the bath, respectively. This formulation is widely adopted to model dynamics of bosonic modes with both noise and extrinsic input/outputs. For example, a beamsplitter-like microwave-optical quantum transducer with independent tunable interaction sites and intrinsic losses could be modeled with

$$\begin{aligned}\frac{d}{dt}\begin{pmatrix} a_m \\ a_o \end{pmatrix} = &- \begin{pmatrix} \frac{\gamma_{\text{ext},m}(t)+\gamma_{\text{int},m}}{2} & ig \\ ig & \frac{\gamma_{\text{ext},o}(t)+\gamma_{\text{int},o}}{2} \end{pmatrix} \begin{pmatrix} a_m \\ a_o \end{pmatrix} \\ &+ \begin{pmatrix} \sqrt{\gamma_{\text{ext},m}(t)}b_{\text{ext},m,\text{in}}(t) + \sqrt{\gamma_{\text{int},m}}b_{\text{int},m,\text{in}}(t) \\ \sqrt{\gamma_{\text{ext},o}(t)}b_{\text{ext},o,\text{in}}(t) + \sqrt{\gamma_{\text{int},o}}b_{\text{int},o,\text{in}}(t) \end{pmatrix}\end{aligned} \tag{2.6}$$

where γ_{ext} are the strengths of the two tunable interactions, γ_{int} are the intrinisic loss strengths, $b_{\text{ext,in}}$ are the lowering operators of the input modes at the two sites, and $b_{\text{in,int}}$ are the lowering operators of the incoming noise modes.

2.2 Quantum State Tomography and Direct Fidelity Estimation

Quantum state tomography, the process of reconstructing a physical quantum state ρ from measurements of the state, is crucial for characterizing quantum hardware [18]. In the simplest scenario, i.e. reproducing a single-qubit density operator, one can repeatedly measure the Pauli operators

$$X = \begin{pmatrix} 0 & 1 \\ 1 & 0 \end{pmatrix}, Y = \begin{pmatrix} 0 & -i \\ i & 0 \end{pmatrix}, Z = \begin{pmatrix} 1 & 0 \\ 0 & -1 \end{pmatrix} \tag{2.7}$$

and reconstruct the state as

$$\rho = \frac{1}{2}\left(I + \langle X\rangle_\rho X + \langle Y\rangle_\rho Y + \langle Z\rangle_\rho Z\right). \tag{2.8}$$

Note that due to measurement projection noise, any finite number of measurements can only reproduce the physical state up to some confidence region, and in some edge cases, the operator reproduced by the linear inversion formula is not positive semidefinite and hence not physical. In general, there are many methods to decide the measurements performed and interpreting the measurement results. The most common approach is maximal-likelihood estimation [19], however, this approach suffers from several numerical caveats, including vanishing eigenvalues and the difficulty of assigning error bars. Variations have been developed to circumvent such issues and integrate better with existing optimization techniques, such as Bayesian inference [20] and adaptive techniques [21].

A major bottleneck of scaling up quantum state tomography is the exponentially grow-

ing Hilbert space dimension. In general, determining an n-qubit state residing in a 2^n-dimensional Hilbert space inevitably encounters the issue of exponential number of parameters to be determined. In particular, to determine an arbitrary physical state residing in a d-dimensional Hilbert space up to ϵ trace distance with no prior information requires at least $\Omega(d^2/\epsilon^2)$ copies of the physical state [22]. To reduce such exponential scaling, many methods have been developed by imposing restrictions to the candidate states, such as low-rank density operators [23], permutationally invariant states [24], matrix product state/operators [25–27], and reduced Boltzmann machines [28]. These methods vastly decrease the number of parameters required to describe candidate states, often to polynomial in the number of physical components, but still describe rich classes of physical states. Another approach, shadow tomography [29], permits determination of an exponential number of measurement expectations with a polynomial number of copies of the physical state, yet requires measurement of a polynomial number of copies simultaneously, limiting its application to near-term quantum hardware.

An alternative tactic to address the exponential scaling dimension problem in the task of quantum state estimation is to limit the number of parameters estimated, such as various entanglement measures. One notable method is classical shadows [30]: inspired by shadow tomography, this method determines exponential number of measurement expectations with a polynomial number of copies of the physical state, but without simultaneous measurements, and in exchange only guarantees accuracy (with high confidence) of any polynomial-sized subset of the measurements. The approach relevant to Chapter 4 is Direct Fidelity Estimation, where the physical state is compared to a predetermined reference pure state, and the parameter extracted is the fidelity between two states [31, 32]. By sampling a complete set of measurements, one can create an unbiased estimate of any operator. For example, for an n-qubit system, since $\mathrm{tr}\,(\rho\sigma) = 2^{-n}\sum_{p\in\mathbb{P}_n}\mathrm{tr}\,(p\rho)\,\mathrm{tr}\,(p\sigma)$, where $\mathbb{P}_n$ is the n-qubit Pauli group, and ρ, σ are n-qubit density operators, to estimate the fidelity between the physical

state ρ and reference pure state σ one can measure p with probability $P(p) = 2^{-n} \left(\mathrm{tr}\left(p\sigma\right)\right)^2$ and estimate the fidelity as

$$\mathrm{tr}\left(\rho\sigma\right) = \sum_{p \in \mathbb{P}_n} P(p) \frac{\mathrm{tr}\left(p\rho\right)}{\mathrm{tr}\left(p\sigma\right)}. \tag{2.9}$$

Similarly, for n-modal bosonic system, $\mathrm{tr}\left(\rho\sigma\right) = \pi^{-n} \int d^n\vec{\alpha} W_\rho(\vec{\alpha}) W_\sigma(\vec{\alpha})$, where $\vec{\alpha}$ is the displacement and $W_\rho(\alpha)$ is the Wigner quasiprobability distribution of ρ at $\vec{\alpha}$, the fidelity can be estimated with $P(\vec{\alpha}) = \pi^{-n} W_\sigma^2(\vec{\alpha})$ and

$$\mathrm{tr}\left(\rho\sigma\right) = \int d^n\vec{\alpha} P(\vec{\alpha}) \frac{W_\rho(\vec{\alpha})}{W_\sigma(\vec{\alpha})}. \tag{2.10}$$

These schemes suffer from potentially vanishing denominators in the weighted averages, hence cutoffs are often applied, i.e. when P is below a preset threshold, the measurement is skipped, leading to a systematic error in the final estimate.

2.3 Stabilizer States of Qudits

2.3.1 Stabilizer Formalism of Qubits

The N-qubit Pauli group is the extension of the single qubit Pauli operators to multiple qubits. It can be defined as

$$\mathbb{P}^N = \langle i, X_{1\ldots N}, Z_{1\ldots N} \rangle, \tag{2.11}$$

note that i is added to include Y. Since $Z_j X_k = (-1)^{\delta_{jk}} X_k Z_j$, we have

$$\left(\prod_j X_j^{x_j} Z_j^{z_j}\right)\left(\prod_k X_k^{x'_k} Z_k^{z'_k}\right) = (-1)^{\vec{z}^T\vec{x}' - \vec{x}^T\vec{z}'} \left(\prod_k X_k^{x'_k} Z_k^{z'_k}\right)\left(\prod_j X_j^{x_j} Z_j^{z_j}\right) \tag{2.12}$$

The phase generated by commutation can be represented as a symplectic bilinear form of a $2N$-dimensional vector space over the ring of integers modulo 2 $\mathbb{Z}_2$, which is also a field:

$$\vec{z}^T\vec{x}' - \vec{x}^T\vec{z}' = \begin{pmatrix}\vec{x}^T & \vec{z}^T\end{pmatrix}\begin{pmatrix}0 & I_N\\ -I_N & 0\end{pmatrix}\begin{pmatrix}\vec{x}'\\ \vec{z}'\end{pmatrix} = \begin{pmatrix}\vec{x}^T & \vec{z}^T\end{pmatrix}\Omega\begin{pmatrix}\vec{x}'\\ \vec{z}'\end{pmatrix} \tag{2.13}$$

Therefore, the normalizer of the Pauli group, the Clifford group, corresponds to symplectic matrices, i.e. each Clifford unitary U corresponds to a matrix M that satisfies $M^T\Omega M = \Omega$, such that

$$U\left(\prod_j X_j^{x_j} Z_j^{z_j}\right)U^\dagger \propto \prod_j X_j^{x'_j} Z_j^{z'_j} \tag{2.14}$$

where $M\begin{pmatrix}\vec{x}\\ \vec{z}\end{pmatrix} = \begin{pmatrix}\vec{x}'\\ \vec{z}'\end{pmatrix}$. Note that under such a definition of Clifford group, it contains the Pauli group as a subgroup, and multiplying any Pauli operator to a Clifford unitary does not change the corresponding symplectic matrix. The single qubit Clifford group is generated by the Hadamard gate $H = \frac{1}{\sqrt{2}}\begin{pmatrix}1 & 1\\ 1 & -1\end{pmatrix}$ and the phase gate $P = \begin{pmatrix}1 & 0\\ 0 & i\end{pmatrix}$. For multiple qubits, an entangling two-qubit Clifford gate, such as the control-not gate $\mathrm{CNOT} = \sum_{j=0}^{1}|j\rangle\langle j|\otimes X^j$ or the control-Z gate $\mathrm{CZ} = \sum_{j=0}^{1}|j\rangle\langle j|\otimes Z^j = \sum_{j,k}(-1)^{jk}|j\rangle\langle j|\otimes|k\rangle\langle k|$, is also required.

A state ρ is described as stabilized by a subgroup of the Pauli group if the state is in the eigenspace of eignevalue 1 for all Pauli operators within the subgroup. An N-qubit pure state $|\psi\rangle$ is a stabilizer state if and only if it is stabilized by a 2^N-element stabilizer group S. For any N-qubit pure stabilizer state, the stabilizer group is of dimension N, and the density operator is the average of all elements in the stabilizer group:

$$|\psi\rangle\langle\psi| = 2^{-N}\sum_{s\in S} s. \tag{2.15}$$

Since the state is represented up to a global phase by the stabilizer group, we can denote the density operator as $|S\rangle\langle S|$.

2.3.2 Stabilizer Formalism of Qudits

For D-level qudits, Pauli matrices are generalized to Weyl–Heisenberg matrices, which is also known as generalized Pauli matrices. The generalized Pauli group is generated by the shift operator $X = \sum_{j=0}^{D-2} |j+1\rangle\langle j| + |0\rangle\langle D-1|$ and the clock operator $Z = \sum_{j=0}^{D-1} e^{2\pi i j/D} |j\rangle\langle j|$. In particular, if D is odd,

$$\mathbb{P}_D^N = \langle X_{1\ldots N}, Z_{1\ldots N} \rangle, \tag{2.16}$$

and if D is even,

$$\mathbb{P}_D^N = \langle e^{\pi i/D}, X_{1\ldots N}, Z_{1\ldots N} \rangle. \tag{2.17}$$

Any generalized Pauli operator can be represented by

$$\omega^\gamma \prod_j X_j^{x_j} Z_j^{z_j} = \omega^\gamma \sigma_\mu, \tag{2.18}$$

where $\omega = e^{2\pi i/D}$, $\mu = \left(\vec{x}^T, \vec{z}^T\right)^T$ and γ is an integer or half-integer representing a global phase. Note that γ can only be a half-integer if D is even, and since $\mathbb{Z}_D$ is a field if and only if D is a prime, μ is considered a vector if and only if D is a prime, and would be a module element otherwise. The commutation relation is given by

$$\left(\prod_j X_j^{x_j} Z_j^{z_j}\right)\left(\prod_k X_k^{x'_k} Z_k^{z'_k}\right) = \omega^{\vec{z}^T\vec{x}' - \vec{x}^T\vec{z}'} \left(\prod_k X_k^{x'_k} Z_k^{z'_k}\right)\left(\prod_j X_j^{x_j} Z_j^{z_j}\right). \tag{2.19}$$

Similarly, generalized Clifford unitaries, the generalization of Clifford unitaries to qudits, correspond to symplectic matrices over $\mathbb{Z}_D$, i.e. for any generalized Clifford unitary U there

exists a symplectic matrix M such that

$$U\sigma_\mu U^\dagger \propto \sigma_{M\mu} \tag{2.20}$$

for any generalized Pauli operator σ_μ. The generalized Clifford group is generated by the phase gate $P = \sum_j \omega^{j^2/2}|j\rangle\langle j|$, generalized Hadamard gate $H = D^{-1/2}\sum_{jk}\omega^{jk}|j\rangle\langle k|$, and either controlled-not CNOT $= \sum_j |j\rangle\langle j| \otimes X^j$ or controlled-Z CZ $= \sum_j |j\rangle\langle j| \otimes Z^j$. An N-qudit pure state is a stabilizer state if and only if stabilized by a D^N-element stabilizer group, and similarly a pure stabilizer state $|\psi\rangle$ is represented by the stabilizer group S up to a global phase, as

$$|\psi\rangle\langle\psi| = D^{-N}\sum_{s\in S} s, \tag{2.21}$$

and the density operator can be denoted as $|S\rangle\langle S|$. For all squarefree D, i.e. the only square number factor of D is 1, the dimension of such stabilizer group is still n, but if D is nonsquarefree, e.g. $D = 4$, the dimension could range from n to $2n$. For example, $\frac{1}{\sqrt{2}}(|0\rangle + |2\rangle)$ is stabilized by $\{I, X^2, Z^2, X^2Z^2\}$, and this group can only be generated by at least two generators. This property of nonsquarefree D stabilizer states will make analysis of these states difficult, and this difficulty is demonstrated in the next subsection.

2.3.3 Bipartite Entanglement of Pure Stabilizer States

Pure stabilizer states always have equal Schmidt coefficients when qudits are grouped into two subsystems, i.e. $\frac{1}{\sqrt{m}}\sum_{j=1}^m |j\rangle \otimes |j\rangle$ for some m. For qubit stabilizer states, this can be proven by analyzing graph states, a special class of stabilizer states where the stabilizer group is generated by a set of stabilizers of the following form:

$$S = \langle X_i \prod_j Z_j^{A_{ij}} \rangle \tag{2.22}$$

where A_{ij} is the adjacency matrix of the N-vertex graph to which the state corresponds. When the N qubits are split into two subsystems of N_A and N_B qubits respectively, and any Clifford unitaries within each subsystem is permitted, then the rank of the $N_A \times N_B$ adjacency matrix between the two subsystems solely determines the amount of entanglement of the state: edges within a subsystem can be cancelled with CZ, and Gaussian elimination operations of the adjacency matrix can be accomplished with CX, resulting in unentangled qudbts and r copies of EPR pairs, where r is the rank of the $N_A \times N_B$ adjacency matrix. This can be extended to qudits with prime levels, with the only twist being the adjacency matrices would be defined over $\mathbb{Z}_D$ instead of $\mathbb{Z}_2$. It can also be shown that all stabilizer states with prime D can be converted to graph states with only qudit-local Clifford gates, and hence this proves the Schmidt decomposition for all bipartite stabilizer states with prime D. This can also be extended to all squarefree D as $\mathbb{Z}_D$ would have a bijection to the tensor product of $\mathbb{Z}_p$ due to Chinese Remainder Theorem. However, this approach cannot transfer to nonsquarefree D.

For stabilizer states with nonsquarefree D, as mentioned in the previous subsection, the stabilizer group can have more dimension than the qudit count. To address this issue, we propose matrices that reproduce the adjacency matrix for any bipartite graph state, are local-Clifford invariant, and are generated by considering the relations between stabilizers instead of qudits. We denote such matrices as Subsystem Phase Matrices, and the definition will be provided in Section 5.3. Utilizing this formalism, it can be shown that any bipartite stabilizer state can be converted to unentangled qudits and entangled pairs with various strength, i.e. two qudits stabilized by $\langle XZ^a, Z^aX\rangle$ where $a \mid D$, using local unitaries.

CHAPTER 3

RECYCLING REFLECTIONS FOR PERFECT PHOTON CAPTURE

3.1 Introduction

Capturing and emitting flying photonic states are cornerstones of quantum optics, enabling state storage, transfer, transduction, and manipulation in quantum networks and computing platforms [33, 34]. Early theoretical work was established by Cirac et al., proposing quantum state transfer between distant nodes via photon capture in cavities, laying the groundwork for quantum networks [35]. Experimental advances have demonstrated quantum state transfers between matter and light [36–39]. When given infinite capture time, an input shaped to an exponential growth pulse can be captured perfectly [40]. In practice, practical constraints results in uncaptured reflections that degrade fidelity due to finite capture windows and coupling strengths, even with control of both sending and receiving nodes [35], and hence, under such constraints, a perfect transfer of arbitrary single mode state is impossible with a single pass. Similarly, exponential decay pulses cannot be captured with finite coupling strength even in the asymptotic limit due to initial reflections.

To overcome these challenges, we propose a two-pass 'pitch-and-catch' photon capture method that recycles initial reflections to *perfectly* transfer arbitrary pulse in the noiseless regime for exponential decay pulses in the asymptotic limit and finite time frame pulses, and increase the fidelity in the presence of noise. The method can also be used for photon emission, utilizing the first pass's emission to extract the remaining excitation in the second pass within a finite time frame. Section 2 formulates the problem using the quantum Langevin equation. Section 3 derives the theoretical limit of single-pass capture, while Section 4 introduces the two-pass method for arbitrary pulses. Sections 5 and 6 extend the analysis to exponential decay pulses in noiseless and noisy regimes, respectively.

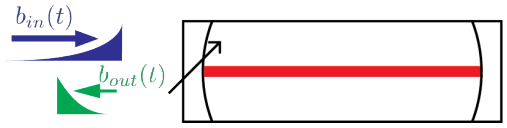

(a) In existing schemes, the input pulse only interacts with the cavity once, leaving a reflection uncaptured.

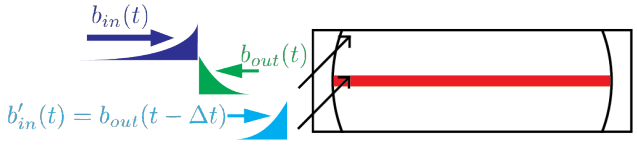

(b) In our proposed scheme, the reflection is redirected back to the cavity after a delay Δt for a second pass of capture.

Figure 3.1: Multiple-pass photon capture

3.2 Methodology

We model photon capture using a quantum Langevin equation for a cavity mode annihilation operator $\hat{a}(t)$ coupled to a traveling mode input $\hat{b}_{in}(t)$ via a tunable coupling $\kappa(t)$, and we analyze the problem in the Heisenberg picture. We assume the cavity starts in a vacuum state, the input state is single-mode, and the system either operates in a linear regime or has at most one excitation, allowing dynamics to be captured by the single-photon wavefunction or equivalently classical amplitudes. Note that such cavity is a visualization of the receiving bosonic mode, and is assumed to be unimodal and in the high-finesse limit. This process can also be applied to non-bosonic devices, such as atomic ensembles in the linear regime, and qubits or atom-cavity systems [35] when the input state has no more than one excitation. The input state is represented by a lowering operator $\hat{c}$, a superposition of $\hat{b}_{in}(t)$, and a corresponding density operator

$$\rho_{in} := \sum_{nm} \frac{\rho_{nm}}{\sqrt{n!m!}} \hat{c}^{\dagger n} |0\rangle\langle 0| \hat{c}^{m}, \tag{3.1}$$

where ρ_{nm} are the density matrix elements defining the input state. The lowering operator of the cavity obeys the following equation:

$$\frac{d}{dt}\hat{a}(t) = -\frac{\kappa(t)}{2}\hat{a}(t) + \sqrt{\kappa(t)}\hat{b}_{in}(t). \tag{3.2}$$

In this regime, the process corresponds to a beamsplitter operation between the cavity and input mode, and $\hat{a}(t)$ is a superposition of $\hat{a}(0)$, $\hat{c}$, and a superposition of $\hat{b}(t')$ orthogonal to $\hat{c}$. Since $\hat{a}(0)$ starts in the vacuum state and the input is unimodal, the commutator $[\hat{a}(t), \hat{c}^\dagger] = a(t)$ is a scalar, which can be interpreted as the complex amplitude of $\hat{a}(t)$ projected in $\hat{c}$. This complex amplitude completely quantifies the efficiency of this capture process, since we have $\left[\hat{c} - a^*(t)\hat{a}(t), \hat{a}^\dagger(t)\right] = a^*(t) - a^*(t) = 0$, so if we let $\hat{c} - a^*(t)\hat{a}(t) = \sqrt{1-|a|^2}\hat{a}'(t)$, where $\hat{a}'(t)$ is orthogonal to $\hat{c}$ and is a superposition of $\hat{b}_{in}(t' > t)$ and $\hat{b}_{out}(t' < t)$, then

$$\rho_a(t) = \mathrm{tr}_{\hat{a}'(t)}\left(\sum_{nm}\frac{\rho_{nm}}{\sqrt{n!m!}}\hat{c}^{\dagger n}|0\rangle\langle 0|\hat{c}^m\right), \tag{3.3}$$

as $\hat{a}(0)$ started with vacuum and the input is unimodal. Hence, we only need to track the commutator between the relevant lowering operators and the raising operator of the input pulse, e.g. $b_{in}(t) = \left[\hat{b}_{in}(t), \hat{c}^\dagger\right]$. $b_{in}(t)$ is the input pulse shape, i.e. $\hat{c}^\dagger = \int b_{in}(t)\hat{b}^\dagger_{in}(t)dt$, but here we interpret it as the complex amplitude of $\hat{b}_{in}(t)$ projected in $\hat{c}$. Note that the t dependence here does not arise from time-dependent dynamics of a mode like $a(t)$ from $\hat{a}(t)$, but a time-dependent label of an infinite family of orthogonal modes $\hat{b}_{in}(t)$. The problem is then reduced to optimizing $\kappa(t)$ to capture an input photon represented by the normalized pulse $b_{in}(t)$, and this work focuses on extending the analysis to two-pass configurations with delayed reflection (see FIG. 3.1). Such cavity obeys the following equation:

$$\begin{aligned}\frac{d}{dt}a(t) = &-\frac{\kappa_1(t)}{2}a(t) + \sqrt{\kappa_1(t)}b_{in}(t) \\ &-\frac{\kappa_2(t)}{2}a(t) + \sqrt{\kappa_2(t)}b'_{in}(t),\end{aligned} \tag{3.4}$$

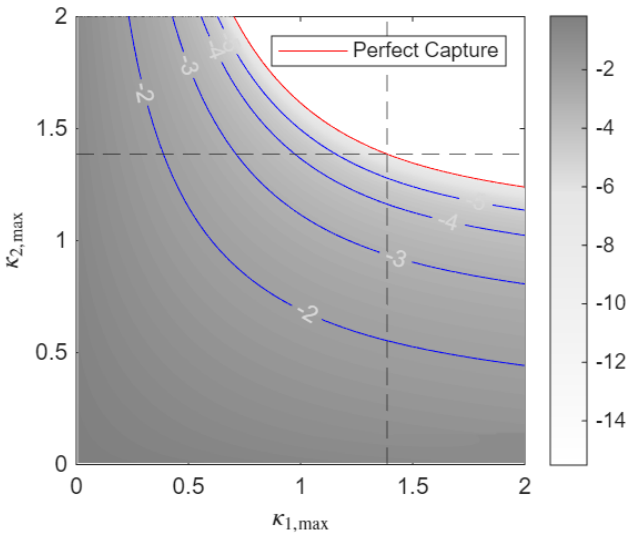

Figure 3.2: Logarithm of minimum loss achievable with two-pass capture for square pulse $\log_{10}(1 - a_{\max}^2)$, where $a_{\max} = \max_{\kappa_1,\kappa_2} a(t = 2b_{\max}^{-2})$. White region corresponds to perfect capture. Dashed line indicates $\kappa = 2\ln 2$, the minimum $\kappa_{\max}$ required to achieve perfect capture when $\kappa_{1,\max} = \kappa_{2,\max} = \kappa_{\max}$. $\kappa_{1,\max}$ and $\kappa_{2,\max}$ are in the units of $b_{\max}^2$.

where

$$b'_{in}(t) = b_{out}(t - \Delta t) = b_{in}(t - \Delta t) - \sqrt{\kappa_1(t - \Delta t)}a(t - \Delta t), \tag{3.5}$$

is the redirected reflection and Δt is the delay for the reflection to reach the cavity again, which we assume to be controllable. Note that $\hat{b}'_{in}$ is in a mode orthogonal to $\hat{b}_{in}$, and κ_2 is controllable independently of κ_1.

3.3 Single Pass Limit

Given a cavity mode a and input pulse b_{in}, the dynamics of the cavity mode is as follows:

$$\frac{da}{dt} = -\frac{\kappa}{2}a + \sqrt{\kappa}b_{in}, \tag{3.6}$$

where t is time and κ is the coupling strength. We want to capture a pulse, which we assume that can be shaped arbitrarily, with a maximal coupling strength $\kappa_{\max}$ within a capture window $t_{\max}$. We reparametrize the equation with $\beta = \kappa^{-1/2}b_{in}$ and $\tau = \int_0^t dt'\kappa(t')$ to

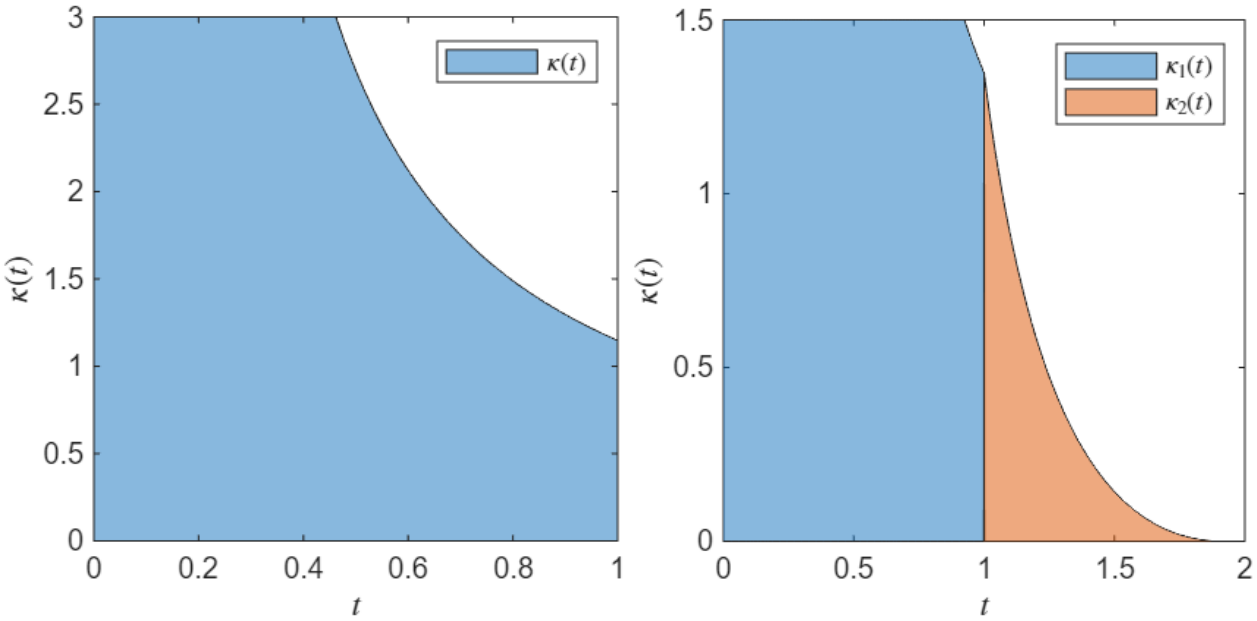

(a) Single-pass $\kappa(t)$ (b) Two-pass $\kappa(t)$

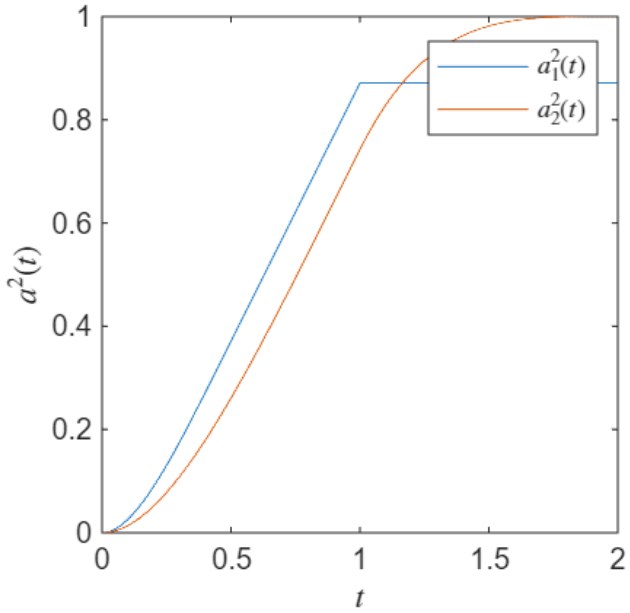

(c) $a^2(t)$ for both schemes

Figure 3.3: Example pulse of single-pass with $\kappa_{\max} = 3b_{\max}^2$ and two-pass capture with $\kappa_{1,\max} = \kappa_{2,\max} = 1.5b_{\max}^2$, and the corresponding efficiency $a^2(t).\kappa(t), \kappa_1(t)$ and $\kappa_2(t)$ are in the units of $b_{\max}^2$, while t is in the units of $b_{\max}^{-2}$.

simplify the dynamics. Hence $\tau_{\max} = \int_0^{t_{\max}} dt' \kappa(t') \leq \kappa_{\max} t_{\max}$. The resultant equation is

$$\frac{da}{d\tau} = -\frac{1}{2}a + \beta, \tag{3.7}$$

and solving it results in

$$a(\tau_{\max}) = \int_0^{\tau_{\max}} d\tau e^{(\tau-\tau_{\max})/2}\beta(\tau). \tag{3.8}$$

Hence, the change of $a(\tau_{\max})$ under variation of $\beta(\tau)$ is given by the following equation:

$$\delta a(\tau_{\max}) = \int_0^{\tau_{\max}} d\tau e^{(\tau-\tau_{\max})/2}\delta\beta(\tau), \tag{3.9}$$

while the normalization varies as follows:

$$\delta \int_0^{\tau_{\max}} d\tau \beta(\tau)^2 = 2\int_0^{\tau_{\max}} d\tau \beta(\tau)\delta\beta(\tau). \tag{3.10}$$

Therefore, to maximize $a(\tau_{\max})$ after the capture under the constraint of $\int_0^{\tau_{\max}} \beta(\tau)^2 d\tau = 1$, we use Lagrange multipliers, yielding $\beta(\tau) \propto e^{\tau/2}$. Applying normalization gives

$$\beta(\tau) = \frac{e^{\tau/2}}{\sqrt{e^{\tau_{\max}} - 1}}, \tag{3.11}$$

and the maximal amplitude of a would be

$$a(\tau_{\max}) = \int_0^{\tau_{\max}} d\tau \frac{e^{\tau-(\tau_{\max}/2)}}{\sqrt{e^{\tau_{\max}} - 1}} = \sqrt{1 - e^{-\tau_{\max}}}. \tag{3.12}$$

The maximum amplitude is thus $a(t_{\max}) = \sqrt{1 - e^{-\kappa_{\max} t_{\max}}}$, achieved with an exponential growth pulse $b_{in}(t) = \frac{\sqrt{\kappa_{\max}} e^{\kappa_{\max} t/2}}{\sqrt{e^{\kappa_{\max} t_{\max}} - 1}}$ and constant $\kappa(t) = \kappa_{\max}$. However, with finite $t_{\max}$ and $\kappa_{\max}$, residual reflection $e^{-\kappa_{\max} t_{\max}}$ is inevitable for any single-pass process.

3.4 Two-pass capture of arbitrary positive packet with bounded magnitude

As shown in Section 3, single-pass capture leaves a residual reflection $e^{-\kappa_{\max} t_{\max}}$, which we aim to eliminate using a two-pass approach, i.e. allowing the reflection to interact with the cavity again. Such a system would follow a Langevin equation in this form:

$$\frac{d}{dt}a(t) = -\frac{\kappa_1(t)+\kappa_2(t)}{2}a(t) + \sqrt{\kappa_1(t)}b_{in}(t) + \sqrt{\kappa_2(t)}b'_{in}(t). \tag{3.13}$$

Here, $\kappa_1(t)$ and $\kappa_2(t)$ are the tunable couplings for the first and second ports, and $b'_{in}(t) = b_{out}(t-\Delta t)$ is the redirected reflection. In this section, we assume the input pulse is positive and bounded, i.e. $0 < b_{in}(t) < b_{\max}$ for any time t during the packet. Note that if one can tune the phase of coupling, complex pulses can be captured with similar processes. Here we choose the time unit that satisfies $b_{\max} = 1$, i.e. t will be in the units of $b_{\max}^{-2}$ and κ will be in the units of $b_{\max}^2$. Consider the instantaneous energy capture efficiency at time t,

$$\begin{aligned}\frac{\frac{d}{dt}a^2(t)}{b_{in}^2(t)} &= -\kappa_1(t)\frac{a^2(t)}{b_{in}^2(t)} + 2\sqrt{\kappa_1(t)}\frac{a(t)}{b_{in}(t)} \\ &= 1 - \left(1 - \sqrt{\kappa_1(t)}\frac{a(t)}{b_{in}(t)}\right)^2\end{aligned} \tag{3.14}$$

$$\kappa_1(t) = \min\left(\kappa_{1,\max}, \left(\frac{b_{in}(t)}{a(t)}\right)^2\right) \tag{3.15}$$

We can see that this choice corresponds to eliminate reflection if possible, and maximize κ_1 otherwise. The square packet, i.e. $\hat{c} = \int_0^1 \hat{b}_{in}(t)\,dt$, maximizes initial reflection, making it the most challenging case for complete capture. For $\kappa_{1,\max} \leq 2\ln 2$, κ_1 is held at $\kappa_{1,\max}$ throughout the packet, yielding

$$a^2(t=1)\Big|_{\kappa_{1,\max}\leq 2\ln 2} = \frac{4}{\kappa_{1,\max}}\left(1 - e^{-\kappa_{1,\max}/2}\right)^2, \tag{3.16}$$

while for $\kappa_{1,\max} > 2\ln 2$, κ_1 is reduced to $\frac{\kappa_{1,\max}}{1+\kappa_{1,\max}(t-t_1)}$ after $t > t_1 = \frac{2\ln 2}{\kappa_{1,\max}}$, at which the capture process shifts into a reflection-less regime, resulting in

$$a^2\left(t=1\right)\Big|_{\kappa_{1,\max}>2\ln 2} = 1 - \frac{2\ln 2 - 1}{\kappa_{1,\max}}. \tag{3.17}$$

In the second pass, similar to the first pass, κ_2 would be set to

$$\kappa_2(t) = \min\left(\kappa_{2,\max}, \left(\frac{b'_{in}\left(t\right)}{a(t)}\right)^2\right) \tag{3.18}$$

The minimal $\kappa_{2,\max}$ required to completely capture the reflected wavepacket from the first pass would then be

$$\kappa_{2,\max} \geq \begin{cases} \frac{\kappa_{1,\max}}{4\left(1-e^{-\kappa_{1,\max}/2}\right)^2}, & \text{if } \kappa_{1,\max} \leq 2\ln 2 \\ \left(1 - \frac{2\ln 2 - 1}{\kappa_{1,\max}}\right)^{-1}, & \text{if } \kappa_{1,\max} > 2\ln 2 \end{cases} \tag{3.19}$$

The achievable loss is illustrated by FIG. 3.2. If $\kappa_{1,\max} = \kappa_{2,\max} = \kappa_{\max}$, the minimal $\kappa_{\max}$ required is $2\ln 2$. Hence, for any bounded packet, $\kappa_{\max} \geq 2\ln 2$ would guarantee perfect two-pass capture, while single-pass efficiency could be limited to $1 - O(\kappa_{\max}^{-1})$, demonstrated by FIG. 3.3. Note that in this section, the two passes are performed separately for better visualization, but in principle they can be performed concurrently; for a square pulse of length T, the two-pass capture can be completed within the time frame of the pulse if $\kappa_{\max} \geq \frac{4\ln 2}{T}$.

3.5 Exponential decay packet

Exponential decay pulses, common in quantum optics due to spontaneous emission, provide a practical case study for our method. Similar to the previous section, we choose time unit that satisfies $\gamma = 1$, i.e. t will be in the units of γ^{-1} and κ will be in the units of γ, and

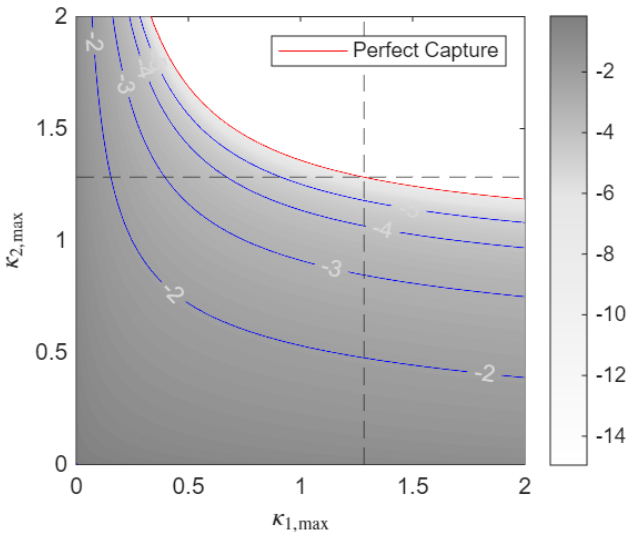

Figure 3.4: Logarithm of minimum loss achievable with two-pass capture for exponential decay pulse $\log_{10}(1-a_{\sup}^2)$, where $a_{\sup} = \sup_{\kappa_1,\kappa_2} \lim_{t\to\infty} a(t)$. White region corresponds to perfect capture. Dashed line indicates $\kappa = k$, the minimum $\kappa_{\max}$ required to achieve perfect capture when $\kappa_{1,\max} = \kappa_{2,\max} = \kappa_{\max}$. $\kappa_{1,\max}$ and $\kappa_{2,\max}$ are in the units of γ.

assume zero intrinsic loss $\kappa_i = 0$. For the exponential decay packet

$$b_{in}(t) = e^{-t/2}, \tag{3.20}$$

equation 3.15 gives a choice of $\kappa_1(t)$ similar to previous section: initially, $\kappa_1(t) = \kappa_{1,\max}$ and reduced to $\frac{\kappa_{1,\max}e^{-t+t_1}}{1+\kappa_{1,\max}\left(1-e^{-t+t_1}\right)}$ for $t > t_1 = \frac{2}{\kappa_{1,\max}-1}\ln\frac{2\kappa_{1,\max}}{\kappa_{1,\max}+1}$, resulting in

$$a_1(t \geq t_1) = e^{-t_1/2}\sqrt{\frac{1}{\kappa_{1,\max}} + 1 - e^{-t+t_1}}. \tag{3.21}$$

With a single pass, the maximal capture efficiency is thus

$$a_1^2(t\to\infty) = \left(\left(1+\kappa_{1,\max}^{-1}\right)^{\kappa_{1,\max}+1}/4\right)^{\left(\kappa_{1,\max}-1\right)^{-1}}, \tag{3.22}$$

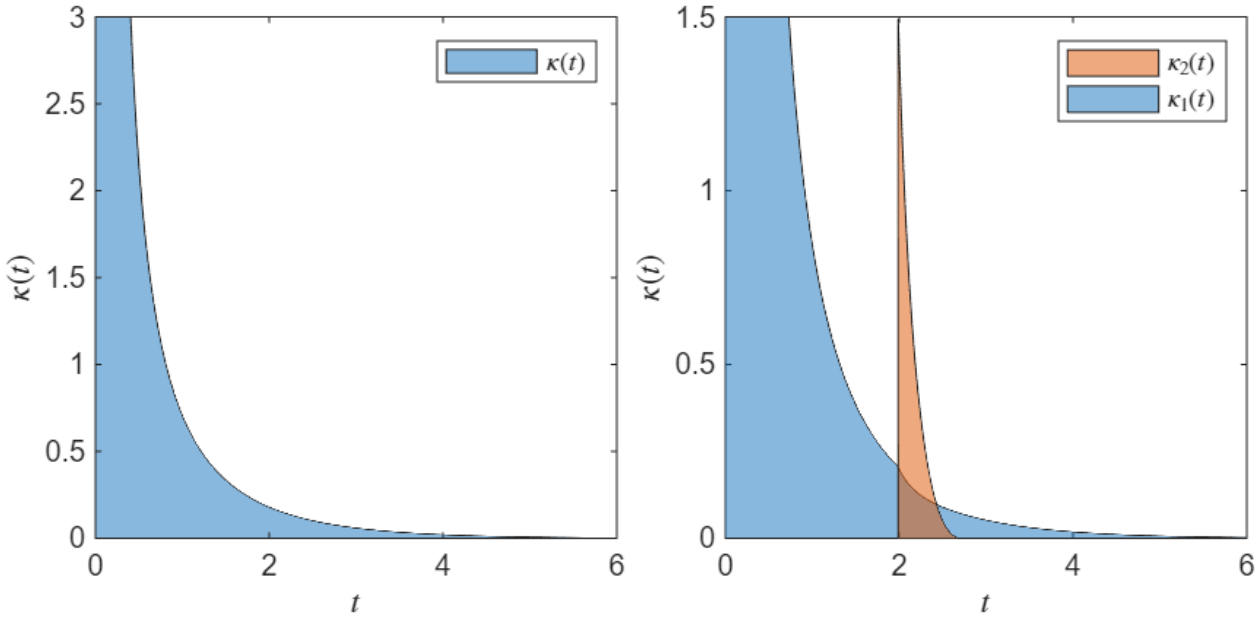

(a) Single-pass $\kappa(t)$ (b) Two-pass $\kappa(t)$

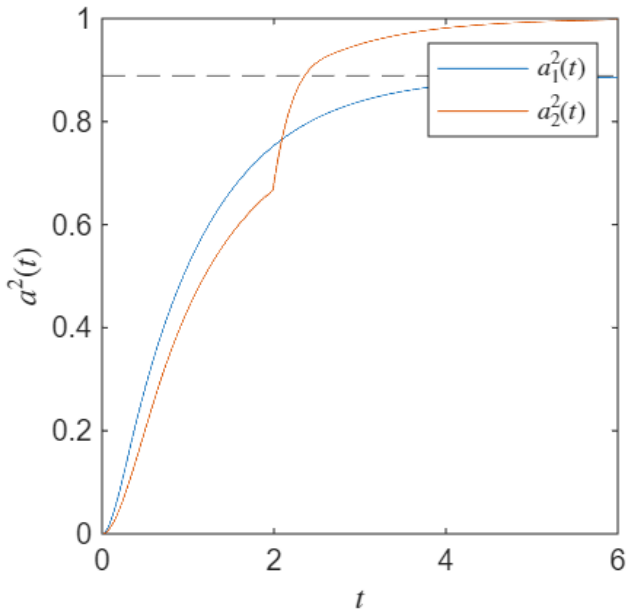

(c) $a^2(t)$ for both schemes

Figure 3.5: Example pulse of single-pass with $\kappa_{\max} = 3\gamma$ and two-pass capture with $\kappa_{1,\max} = \kappa_{2,\max} = 1.5\gamma$, and the corresponding efficiency $a^2(t)$. Dashed line indicates the maximum efficiency of the single-pass scheme in the asymptotic limit. $\kappa(t), \kappa_1(t)$ and $\kappa_2(t)$ are in the units of γ, while t is in the units of γ^{-1}.

which is approximately $1-\frac{2\ln 2-1}{\kappa_{1,\max}}$ for large $\kappa_{\max}$. To make $b'_{out}(t)=0$, it is clear that the maximal κ_2 is only required at $t=\Delta t$, thus

$$1-\sqrt{\kappa_{2,\max}}a(\Delta t)=b'_{out}(\Delta t)=0. \tag{3.23}$$

Therefore, to achieve perfect capture, we must have

$$\kappa_{2,\max}\left(\left(1+\kappa_{1,\max}^{-1}\right)^{\kappa_{1,\max}+1}/4\right)^{\left(\kappa_{1,\max}-1\right)^{-1}}>1. \tag{3.24}$$

Assuming $\Delta t\geq t_1$, we have

$$\sqrt{1+\kappa_{1,\max}\left(1-e^{-\Delta t+t_1}\right)}=\sqrt{\frac{\kappa_{1,\max}}{\kappa_{2,\max}}}e^{t_1/2} \tag{3.25}$$

$$\Delta t=t_1+\ln\frac{1}{1+\kappa_{1,\max}^{-1}-\kappa_{2,\max}^{-1}e^{t_1}}. \tag{3.26}$$

In other words, if $\kappa_{2,\max}>\kappa_{1,\max}e^{t_1}$, one can start capturing the reflection before the first pass reaches reflectionless regime. If $\kappa_{1,\max}=\kappa_{2,\max}=\kappa_{\max}$, the infimal $\kappa_{\max}$ required to achieve perfect capture is $\kappa_{\max}>k\approx 1.2834$, where k satisfies $(k+1)^{k+1}=4k^2$. For example, if $\kappa_{\max}=2$, then $\Delta t=\ln\frac{32}{11}$, while if $\kappa_{\max}>>1$, then $\Delta t\approx t_1\approx\frac{2\ln 2}{\kappa_{\max}}$. The achievable minimal loss is illustrated in FIG. 3.4.

$$b_{out}(0\leq t\leq t_1)=\frac{2\kappa_{1,\max}}{\kappa_{1,\max}-1}e^{-\kappa_{\max}t/2}-\frac{\kappa_{1,\max}+1}{\kappa_{1,\max}-1}e^{-t/2} \tag{3.27}$$

$$\kappa_1(t>t_1)=\left(\frac{b_{in}(t)}{a_2(t)}\right)^2,\kappa_2(t\geq\Delta t)=\left(\frac{b'_{in}(t)}{a_2(t)}\right)^2 \tag{3.28}$$

$$a_2^2(t>\Delta t)=a^2(\Delta t)+\int_{\Delta t}^{t}\left(b_{in}^2\left(t'\right)+b_{in}'^2\left(t'\right)\right)dt' \tag{3.29}$$

Thus, in the asymptotic limit, the two-pass method eliminates the loss of $O(\gamma/\kappa_{\max})$ as long as $\kappa_{\max}/\gamma > k$ in the noiseless regime, demonstrated by FIG. 3.5.

3.6 Exponential decay packet with intrinsic loss

Intrinsic loss κ_i models dissipation in the cavity and delay line, reducing capture efficiency. For simplicity, assume $\kappa_{i,cav} = \kappa_{i,delay} = \kappa_i \ll \kappa_{1,\max}, \kappa_{2,\max}, \gamma$. (If $\kappa_{i,cav} > \kappa_{i,delay}$, the solution would involve actively sending amplitude into the delay line; conversely, if $\kappa_{i,cav} < \kappa_{i,delay}$, the solution would involve premature second capture.) In such case, the zero reflection still provides the optimal solution, except both single and double capture will have an optimal stop time. Similar to the previous section, we choose time unit that satisfies $\gamma = 1$, i.e. t will be in the units of γ^{-1} and κ will be in the units of γ, and let $\alpha = \frac{1-\kappa_i}{\kappa_{1,\max}}$. For the initial stage of the capture:

$$a(t \le t_1) = \frac{2e^{-t/2}}{(1-\alpha)\sqrt{\kappa_{1,\max}}} \left(1 - e^{-(1-\alpha)\kappa_{1,\max} t/2}\right) \tag{3.30}$$

After $t > t_1 = \frac{2}{(1-\alpha)\kappa_{1,\max}} \ln \frac{2}{1+\alpha}$, the reflection can be eliminated, resulting in

$$a_1(t \ge t_1) = \left(\alpha\kappa_{1,\max}\right)^{-1/2} e^{-t/2} \sqrt{(1+\alpha)\, e^{\alpha\kappa_{1,\max}(t-t_1)} - 1} \tag{3.31}$$

We can now solve for maximal capture efficiency for the single-pass capture, which occurs at

$$T_1 = t_1 - \frac{\ln\left(\kappa_i(1+\alpha)\right)}{\alpha\kappa_{1,\max}} \tag{3.32}$$

$$= \frac{2\alpha\ln 2 - (1-\alpha)\ln\kappa_i - (1+\alpha)\ln(1+\alpha)}{\alpha\kappa_{1,\max}(1-\alpha)} \tag{3.33}$$

with the final efficiency of

$$a_1^2(T_1) = \kappa_i^{\frac{\kappa_i}{1-\kappa_i}} 2^{-\frac{2}{\kappa_{1,\max}+\kappa_i-1}} (1+\alpha)^{\frac{1+\alpha}{\alpha\kappa_{1,\max}(1-\alpha)}} \tag{3.34}$$

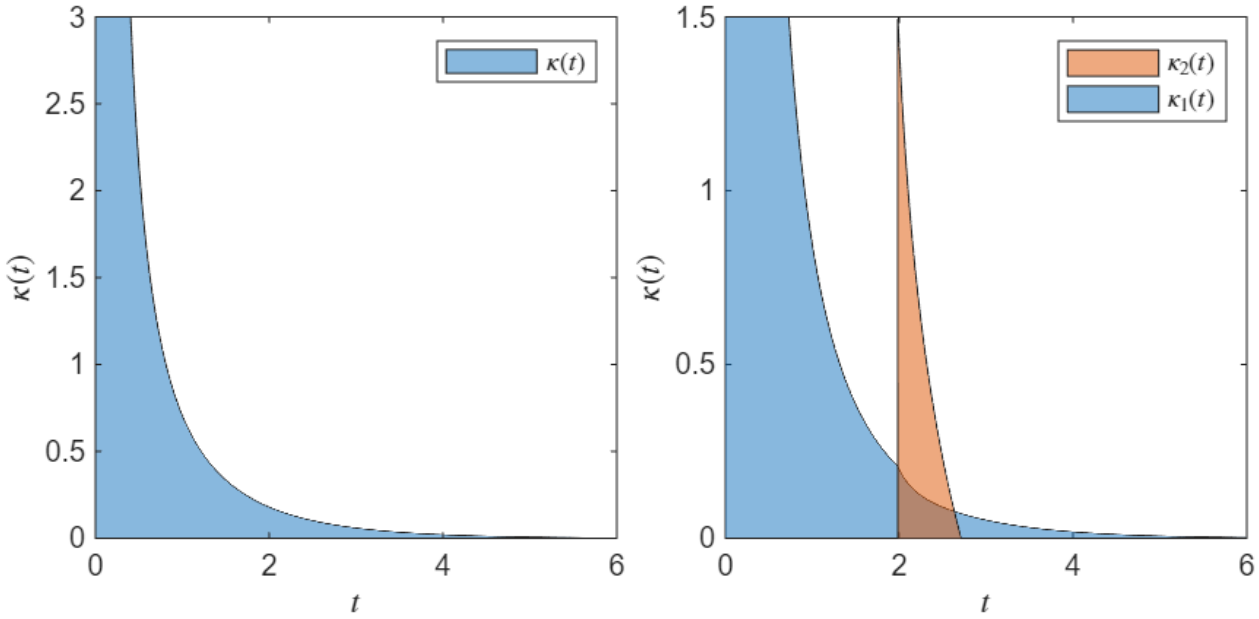

(a) Single-pass $\kappa(t)$ (b) Two-pass $\kappa(t)$

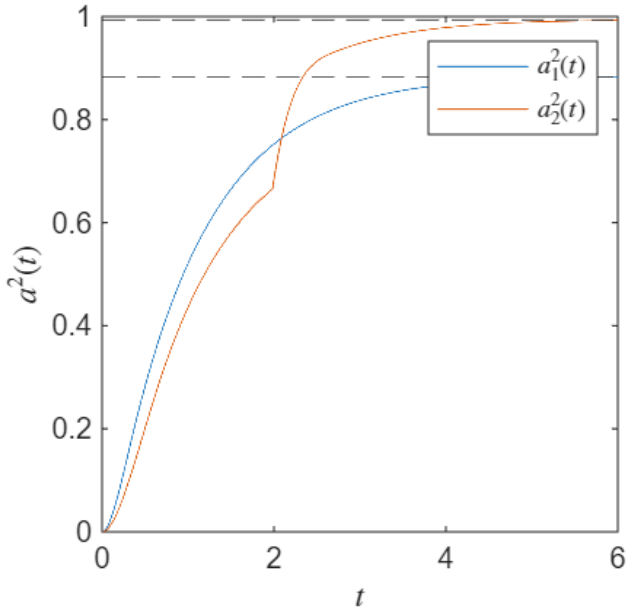

(c) $a^2(t)$ for both schemes

Figure 3.6: Example pulse of single-pass with $\kappa_{\max} = 3\gamma$ and two-pass capture with $\kappa_{1,\max} = \kappa_{2,\max} = 1.5\gamma$, and the corresponding efficiency $a^2(t)$, with intrinsic loss $\kappa_i = 0.001\gamma$. Dashed lines indicates the achievable maximum efficiencies of the two schemes. $\kappa(t), \kappa_1(t)$ and $\kappa_2(t)$ are in the units of γ, while t is in the units of γ^{-1}.

For the two-pass capture, once again assuming $\Delta t \geq t_1$, we delay the recapture of reflection by

$$\Delta t = t_1 + (\alpha\kappa_{1,\max})^{-1} \ln \frac{1}{1+\alpha-\alpha\kappa_{1,\max}\kappa_{2,\max}^{-1} e^{\alpha\kappa_{1,\max}t_1}} \tag{3.35}$$

such that

$$\sqrt{\kappa_{2,\max}}a(\Delta t) = b'_{in}(\Delta t) = e^{-\kappa_i \Delta t/2} \tag{3.36}$$

Similar to the previous section,

$$\frac{\kappa_{2,\max}}{\alpha\kappa_{1,\max}} \left(\frac{(1+\alpha)^{\alpha^{-1}+1}}{4} \right)^{(\alpha^{-1}-1)^{-1}} > 1 \tag{3.37}$$

is required for 0 reflection at Δt, which reduces to $\alpha^{-1} > k \approx 1.2834$ if $\kappa_{1,\max} = \kappa_{2,\max} = \kappa_{\max}$. Applying this assumption, Δt reduces to

$$\Delta t = t_1 + (\alpha\kappa_{1,\max})^{-1} \ln \frac{1}{1+\alpha-\alpha e^{\alpha\kappa_{1,\max}t_1}} \tag{3.38}$$

and the capture efficiency is

$$\begin{aligned} a_2^2(t) = &\frac{e^{-\kappa_i t} - e^{-t}}{1-\kappa_i} \\ &- \int_{t-\Delta t}^{t_1} \left(e^{-t'/2} - \sqrt{\kappa_{1,\max}}a(t') \right)^2 e^{-\kappa_i(t-t')} dt' \end{aligned} \tag{3.39}$$

for $\Delta t \leq t \leq \Delta t + t_1$, and

$$a_2^2(t) = \frac{e^{-\kappa_i t} - e^{-t}}{1-\kappa_i} \tag{3.40}$$

if $t \geq \Delta t + t_1$. Hence,

$$T_2 = -\frac{\ln \kappa_i}{\alpha\kappa_{1,\max}}, \tag{3.41}$$

resulting with

$$a_2^2(T_2) = \kappa_i^{\frac{\kappa_i}{1-\kappa_i}} \tag{3.42}$$

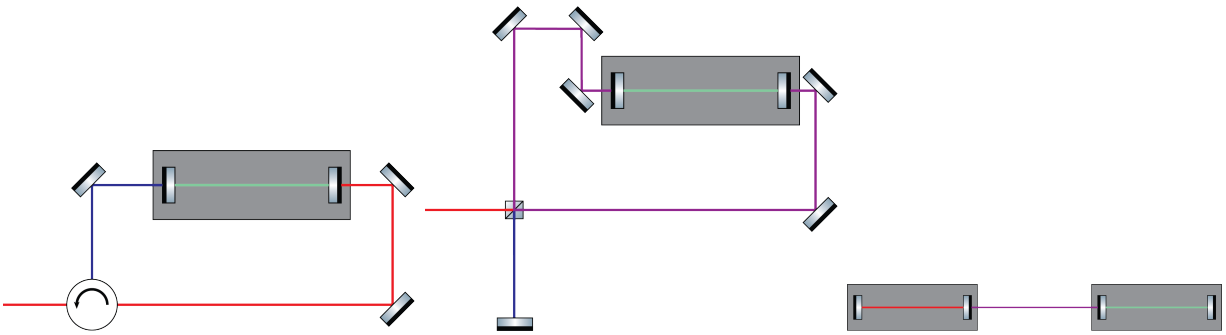

(a) Circulator-based setup (b) Michelson-like setup (c) Back-and-forth setup

Figure 3.7: Various setups for achieve two-pass capture. In 3.7a, the reflection from the right port is redirected to the left port via a circulator, which can be implemented with non-reciprical optical components, such as a Faraday isolator. In 3.7b, two branches differs by $\frac{\pi}{2}$, hence when the reflection reaches the beamsplitter, one branch accumulates an extra π phase, and the reflection will reach the mirror and be redirected to the cavity again instead of the source. In 3.7c, the reflection is utilized by the source cavity to extract the remaining excitations, then back to the destination cavity for the second-pass capture. Any reabsorption by the source cavity will be reemitted back to the destination cavity.

Note that we assumed $T_2 > \Delta t + t_1$, which requires

$$\kappa_i \leq (1+\alpha)\left(\frac{1+\alpha}{2}\right)^{4\alpha/(1-\alpha)} - \frac{\alpha\kappa_{1,\max}}{\kappa_{2,\max}}\left(\frac{1+\alpha}{2}\right)^{2\alpha/(1-\alpha)}. \tag{3.43}$$

For example, if $\kappa_{\max} = 2$, $\kappa_i \lesssim 0.225$. The two-capture process eliminated a factor of $a_1(T_1)/a_2(T_2) = \left(2^{-(1-\alpha)^{-1}}(1+\alpha)^{(1-\alpha)^{-1}+1/(2\alpha)}\right)^{\kappa_{1,\max}^{-1}}$, which is approximately $1 - \frac{\gamma}{\kappa_{1,\max}}\ln\frac{2}{\sqrt{e}}$ for small α, and now the capture efficiency is now $1 - \widetilde{O}(\frac{\kappa_i}{\gamma})$, only limited by the ratio between intrinsic loss and decay rate of the input pulse, demonstrated in FIG. 3.6. The overall capture time is also slightly shortened.

3.7 Discussion

The two-pass method significantly enhances photon capture over single-pass approaches by leveraging reflected pulses. Unlike single-pass methods, our two-pass method achieves perfect transfer for arbitrary pulses when $\frac{\kappa_{\max}}{\max_t b_{in}(t)} \geq 2\ln 2$ in the noiseless regime, and eliminates

the $e^{-O(\gamma/\kappa_{\max})}$ factor in capture efficiency in the noisy regime. Compared to prior single-pass techniques, our approach offers higher fidelity in realistic noisy conditions, providing potential improvements to quantum repeaters and memory nodes in quantum networks.

Current systems, both in optical and microwave regimes, are capable of shaping and capturing traveling photonic packets of timescales much shorter than the cavity intrinsic decays [39, 41, 42]. By applying our scheme, the reflection loss can be further reduced. There are many possible setups (refer to FIG. 3.7) to redirect the reflection back to the cavity in an orthogonal mode, including (a) optical circulator, (b) Michelson-like setup, and depending on the setup one can even just (c) utilize the reflection to extract the remaining excitation from the source. By reversing the process, our method can also be used to release arbitrarily shaped pulses, enhancing its utility for quantum pulse shaping. For quantum state transfer, our scheme can thus reduce both residual and reflection loss. Future work could explore thermal noise, non-linearity, alternative initial cavity state, designs for experimental implementations and multimode extensions.

3.8 Conclusion

Our two-pass method surpasses single-pass limitations, achieving perfect capture of arbitrary pulses in ideal conditions and superior fidelity with noise, advancing photonic manipulation for quantum technologies. These findings advance the toolkit for photonic state manipulation in quantum information systems.

CHAPTER 4

EFFICIENT QUANTUM TOMOGRAPHY OF A POLYNOMIAL SUBSPACE

4.1 Introduction

Due to the exponentially large dimension of its Hilbert space, a complete characterization of an arbitrary state in a multipartite quantum system is intractable: for an m-partite system, with each part having n local dimensions, the Hilbert space dimension is n^m. In addition, noise during evolution can decohere the quantum system and lead to a mixed state in the end. Therefore, we must generally use density matrices to describe the states, further increasing the number of parameters that must be estimated. Hence, a full tomography requires determining $n^{2m} - 1$ real parameters, which means that the number of identical copies of the system needed to be prepared grows exponentially as the number of parties increases. Therefore, the tomography task is usually impractical for large m due to resource consumption.

To be more resource-efficient for state characterization, additional constraints on the states' form or the system's structure are needed. For example, if the density matrices have a low rank, compressed sensing techniques can be applied to reduce sample complexity [23, 43]. Efficient methods to do tomography using matrix product states (MPS) [25, 26] or matrix product operators (MPO) [27, 44], which are often related to 1D systems with local interaction, have also been developed. It is also possible to use an adaptive method [45, 46] or even machine learning protocols [47, 48] to optimize the measurement basis chosen.

There are also approaches that avoid tomography completely: If preparation of the desired state is assumed to be as accurate as possible, one can apply direct fidelity estimation (DFE) with the ideal state, using an importance sampling rule [31, 32] to verify the state rather than performing a full tomography. However, encountering vanishing weights in the

“importance-weighting" rule introduced in previous works can lead to a significant increase in sampling overhead. Addressing this issue requires the use of cutoffs, which in turn introduces systematic errors. Moreover, previous methods are limited to estimating the overlap with pure states. Concurrent with this work, multiple works have optimized the sampling rule [49–51], and Guo et. al. [51] extended to estimating expected value of operators.

In many situations, the physical state is expected to exist in a confined subspace whose dimension scales polynomially rather than exponentially with the number of parties. For example, the state could be in a subspace where engineered dissipation or a blockade Hamiltonian constrains the dynamics [52–54]. Additionally, if the state preparation noise is small, one would expect the resultant state to be within a neighborhood of the target state, which we formalize later. However, states in such a subspace could be highly entangled and difficult to characterize or verify.

In this manuscript, we establish a subspace tomography method, Direct Extraction of Density Matrix Elements from Subspace Sampling Tomography (DEMESST): we provide a systematic method to generate a physically relevant polynomial-dimensional subspace, generalize and optimize DFE to estimate arbitrary operator with arbitrary spanning set of measurements, then apply the generalized DFE to obtain estimates of expected values of elements within the subspace to reconstruct the projected density operator.

Section 4.2 summarizes the efficiency of generalized DFE to estimate various classes of states, section 4.3 describes the method to generate the physically relevant subspace, section 4.4 derives the generalized DFE, and section 4.5 contains examples of applying generalized DFE to various states with various sets of measurements.

4.2 Summary of results

The results are summarized in TABLES 4.1 & 4.2, representing the maximum DFE overhead of certain families of states with certain measurements. Each column represents the base

<table>
<tr><th>Maximum DFE Cost / States / Measurements</th><th>Stabilizer State (Corollary 2)</th><th>Product State (Corollary 4)</th><th>Matrix Product State (bond dimension $k = O(1)$) (Corollary 5)</th><th>Arbitrary Pure State (Corollary 1)</th></tr>
<tr><td>Pauli Measurements</td><td rowspan="4">$\leq 2 - 2^{1-m}$</td><td colspan="3">$2^{\Theta(m)}$</td></tr>
<tr><td>Product Measurements</td><td rowspan="3">1</td><td rowspan="3">$2^{O(n)}$</td></tr>
<tr><td>Product Measurements with $O(m)$ Quasilocal Gates and $O(1)$ Ancilla Qubits</td></tr>
<tr><td>Arbitrary Measurements</td></tr>
<tr><td>LOCC (if conjecture 1 holds)</td><td colspan="4">$\leq 2 - 2^{1-m}$</td></tr>
</table>

Table 4.1: Summary of DFE cost $Z_{\mathcal{M}}$ of multiqubit states with sets of measurements $\mathcal{M}$. A value of $Z_{\mathcal{M}} = 1$ indicates that the projection of the state can be implemented perfectly within $\mathcal{M}$, while $2 - 2^{1-m}$ is usually achieved by a set of traceless measurements such that the (weighted) average is proportional to the projector of the state, up to a constant deviation. Blue entries indicate that we do not have tight proven bounds yet: $2^{O(n)}$ is just a trivial upper bound, while $2 - 2^{1-m}$ for arbitrary pure state with LOCC measurements depends on a conjecture. Note that a state do not need to be strictly in a category for it to be in the neighbourhood of such category, refer to Section 4.2 and Theorem 1 for details.

<table>
<tr><th>Maximum DFE Cost
Measurements \ States</th><th>GKP State (Corollary 3)</th><th>Coherent State</th><th>Product State (Corollary 4)</th><th>Pure Gaussian State (Corollary 6)</th><th>Arbitrary Pure State (Corollary 1)</th></tr>
<tr><td>Parity Measurements with Displacement</td><td rowspan="3">2</td><td colspan="3" rowspan="2">$2^{\Omega(m)}$</td><td rowspan="2"></td></tr>
<tr><td>Parity Measurements and Vacuum Projections with Displacements</td></tr>
<tr><td>Product Measurements</td><td colspan="2" rowspan="3">1</td><td rowspan="2"></td><td rowspan="3">?</td></tr>
<tr><td>Product Measurements with Gaussian Unitaries</td><td rowspan="2"></td></tr>
<tr><td>Arbitrary Measurements</td><td></td></tr>
<tr><td>LOCC (if conjecture 1 holds)</td><td colspan="5">≤ 2</td></tr>
</table>

Table 4.2: Summary of DFE cost of multimode bosonic states. 1 indicates that the projector can be achieved directly, while 2 is usually achieved with a (weighted) average of traceless measurements. Once again, blue entries indicate we do not have tight proven bounds yet.

state of a neighborhood subspace, while each row represents the available measurements. Diagonal entries are proved in the following sections as corollaries. If an entry is constant, then the neighborhood generated from a base state of that category with local operators allows efficient tomography with the corresponding set of measurements. Note that a state σ does not need to be in the category itself to allow efficient neighborhood tomography. For example, a W state itself is not a product nor a stabilizer state. However, being the equal superposition of the states resulting from applying X of different qubits on $|0\rangle^{\otimes m}$, it is considered to be in the neighborhood of the $|0\rangle^{\otimes m}$ state. Since $|0\rangle^{\otimes m}$ is a product state and a stabilizer state, it has a constant overhead, as shown in the table. Hence, the DFE overhead of a W state is at most polynomial in m for all listed measurement sets. The second column of TABLE 4.2 has been experimentally demonstrated by performing tomography in a bounded photon subspace in up to four modes of a multimode bosonic system [6].

4.3 Polynomial neighborhood subspace

In many situations, we expect the state prepared in an experiment to only slightly differ from a target pure state. To formalize this, we define the neighborhood subspace of a pure state as follows.

Definition 1. Given a pure state $|\psi\rangle$ and a set of operators $\mathcal{K}$, define the neighborhood of $|\psi\rangle$ generated by $\mathcal{K}$ k times iteratively as

$$N_0(|\psi\rangle, \mathcal{K}) = span(\{|\psi\rangle\}), \tag{4.1}$$

$$\begin{aligned} N_{k+1}(|\psi\rangle, \mathcal{K}) = span(\{K|\psi'\rangle \,|\, K \in \{I\} \cup \mathcal{K}, \\ |\psi'\rangle \in N_k(|\psi\rangle, \mathcal{K})\}). \end{aligned} \tag{4.2}$$

For example, if we prepare some state $|\psi\rangle$ and allow it to evolve under some Lindbladian $\mathcal{L}(\rho) = \gamma \sum_i (L_i \rho L_i^\dagger - \frac{1}{2}\{L_i^\dagger L_i, \rho\})$ for a short time $t \ll \gamma^{-1}$, we would expect most of the

state to end up within $N_k(|\psi\rangle, \cup_i \{L_i, L_i^\dagger L_i\})$, i.e.

$$\mathrm{tr}\left(\Pi_k \rho_t \Pi_k\right) = 1 - O\left((\gamma t)^{k+1}\right),$$

where Π_k is the projection operator onto N_k. Such spaces have dimensions polynomial in $|\mathcal{K}|$ regardless of the dimension of the complete Hilbert space:

Lemma 1. *The dimension of the neighborhood generated from a pure state $|\psi\rangle$ ("base state") with at most k applications of a combination of operators from $\mathcal{K}$ is polynomial in $|\mathcal{K}|$ if $k = O(1)$.*

Proof.

$$\dim\left[N_0(|\psi\rangle, \mathcal{K})\right] = 1, \tag{4.3}$$

$$\begin{aligned} \dim\left[N_k(|\psi\rangle, \mathcal{K})\right] &\leq (|\mathcal{K}| + 1) \dim\left[N_{k-1}(|\psi\rangle, \mathcal{K})\right] \\ &\leq (|\mathcal{K}| + 1)^k. \end{aligned} \tag{4.4}$$

□

Hence, the exponential dimension of the entire Hilbert space does not inhibit partial tomography of the relevant subspace. As an example, the tomography of any polynomial dimensional subspace $\mathcal{S}$, which can be seen as a neighborhood subspace generated from a pure state $|\psi\rangle \in \mathcal{S}$ with $\dim(\mathcal{S}) - 1$ different unitaries, is possible if arbitrary measurements are allowed:

Corollary 1. *If arbitrary (multipartite) measurements are allowed, tomography of any subspace $\mathcal{S}$ within ϵ Frobenius distance with at least $1 - \delta$ success probability can be performed in* $\mathrm{poly}(\dim \mathcal{S}, \epsilon, \ln \delta^{-1})$ *measurements.*

Proof. By choosing an orthonormal basis $\{|\psi_l\rangle\}$ of $\mathcal{S}$, we only need to treat the system as a $(\dim \mathcal{S})$-level qudit and perform standard tomography to retrieve the projected density operator. Note that the resultant operator should not be renormalized to unit trace because

the physical state may not entirely lie within this subspace, and this procedure only retrieves the projected state. This is listed as the final column in TABLES 4.1 & 4.2. □

However, arbitrary measurements are hard to implement. Therefore, in the following, we present a method to realize this tomography with available measurements.

4.4 Generalized direct fidelity estimation

To build a method for performing tomography in some d-dimensional subspace, which corresponds to estimating the expectations of a linearly independent set of d^2 Hermitian operators, we need the capability to effectively estimate the expectation of an arbitrary Hermitian operator in the subspace. DFE can be regarded as a special case with $d = 1$, where the overlap of two states is sampled with certain families of measurements, such as Pauli measurements and Wigner measurements. For example, one can write the overlap of two states as the inner product of the vectors of expectation values of such measurable operators and estimate it by sampling the ratio of expected value with the reference value squared as the probability function [31, 32]. In particular, to obtain the overlap between some known m-qubit pure state $\sigma = |\psi\rangle\langle\psi|$ and some unknown m-qubit physical state ρ, one can perform DFE to estimate $\mathrm{tr}\,(\rho\sigma) = 2^{-m}\sum_{P\in\mathcal{P}}\mathrm{tr}\,(P\rho)\,\mathrm{tr}\,(P\sigma) = \sum_{P\in\mathcal{P}} p_P \frac{\mathrm{tr}\,(P\rho)}{\mathrm{tr}\,(P\sigma)}$, where $\mathcal{P} = \{I, X, Y, Z\}^{\otimes m}$ is a subset of the Pauli group, and $p_P = 2^{-m}\left(\mathrm{tr}\,(P\sigma)\right)^2$. Note that p_P does not depend on ρ and is determined before the measurements. Such methods suffer from statistical and/or systematic errors induced by small denominators when some of the reference values have small magnitudes.

To address the vanishing denominator problem, we propose optimizing the choice of sampling probability and adjusting the weight of each measurement accordingly. For simplicity, we assume that the operator we measure is Hermitian, and all possible measurement operators have only measurement results of ± 1. We can express the expectation value of any Hermitian operator $\mathcal{O}$ within the subspace spanned by the identity and the available

measurement operators, as a weighted sum of the expectation values of measurements:

$$\langle \mathcal{O} \rangle_\rho = C(\mathcal{O}) + \sum_i f_i(\mathcal{O}) \operatorname{tr}(M_i \rho), \tag{4.5}$$

where M_i is the i^{th} available measurement, f_i and C are real coefficients dependent on $\mathcal{O}$ and the set of measurement operators, and $\operatorname{tr}(M_i\rho)$ are the expectation values of measurement. In DFE, $\langle \mathcal{O} \rangle_\rho$ is estimated by obtaining the following expected value:

$$\mathbb{E}_i \left[w_i \langle M_i \rangle_\rho \right] = \sum_i p_i w_i \operatorname{tr}(M_i \rho), \tag{4.6}$$

where p_i is the probability of performing measurement M_i and w_i is the weight assigned to the measurement. If $p_i w_i = f_i$, the weighted mean is an unbiased estimator of the overlap. We construct a random variable X via a combination of classical randomness and quantum measurement: for each instance of the variable, we randomly select an i, each with a probability of p_i, then we measure M_i, and assign the measurement outcome multiplied by w_i to X, then we have

$$\mathbb{E}[X] = \langle \mathcal{O} - C \rangle_\rho. \tag{4.7}$$

Note that the randomness of such random variable is a combination of both the classical randomness and the quantum projection noise. For pure reference states $\mathcal{O} = \sigma$, traditional DFE methods [31, 32] have $C = 0$, and use $p_i = f_i(\sigma) \operatorname{tr}(M_i \sigma)$ and $w_i = (\operatorname{tr}(M_i \sigma))^{-1}$. This formulation of p_i and w_i utilizes the fact that $\sum_i f_i(\sigma) \operatorname{tr}(M_i \sigma) = \operatorname{tr}(\sigma^2) = 1$, which implies p_i is a probability distribution. However, as discussed previously, this suffers from potentially divergent fractions, and the application of a cut-off to avoid statistical errors from small denominators induces a systematic error.

In our generalized DFE method, we minimize variance per measurement:

$$\begin{aligned}\mathrm{Var}\left[X\right] &= \mathbb{E}_i\left[w_i^2\right] - \langle \mathcal{O} - C\rangle_\rho^2 = \sum_i p_i |w_i|^2 - \langle \mathcal{O} - C\rangle_\rho^2 \\ &= \sum_i p_i |w_i|^2 \sum_j p_j - \langle \mathcal{O} - C\rangle_\rho^2 \geq \left(\sum_i |f_i|\right)^2 - \langle \mathcal{O} - C\rangle_\rho^2.\end{aligned} \tag{4.8}$$

Due to the Cauchy-Schwarz inequality, the variance is minimized when the equality is satisfied, which requires $p_i|w_i|^2 \propto p_i$. Therefore, all w_i must have the same magnitude, thus $p_i w_i = f_i$ implies $p_i \propto |f_i|$. Hence, we construct the following distribution:

$$\begin{cases} Z(\mathcal{O}) = 2\sum_j |f_j(\mathcal{O})|, \\ w_i(\mathcal{O}) = \dfrac{1}{2}\mathrm{sgn}[f_i(\mathcal{O})] Z(\mathcal{O}), \\ p_i(\mathcal{O}) = \dfrac{2|f_i(\mathcal{O})|}{Z(\mathcal{O})}, \end{cases} \tag{4.9}$$

where Z, twice the sum of all weights, is effectively the overhead of this procedure, as the variance per measurement is upper bounded by $Z^2/4$. When the set of measurements is linearly independent, such as Pauli measurements or Wigner measurements, Z is proportional to 1-norm, matching the results of [49–51]. Since such a distribution eliminates the possibility of small denominators, we eliminate the systematic errors generated by introducing a cutoff for handling small denominators in existing DFE methods. Note that while this approach attains minimal sample complexity over all possible parametrizations of p_i and w_i that satisfy $p_i w_i = f_i$, it does not rule out instances of states with exponential sample complexity. Since the measurement outcomes can only be ± 1, Hoeffding's inequality provides a bound on the sampling complexity that is polynomial in Z, the inverse of tolerable error ϵ, and the logarithm of the failure rate δ.

In principle, we can relax the measurement outcomes to arbitrary real numbers and consider implementations of measurements with POVMs. Note that with such relaxation,

the sampling distribution is no longer guaranteed to be optimal in variance per measurement, as the proof relies on the property that the square of any measurement outcome is 1. If M_i is implemented with POVM $\{\Lambda_j^{(i)}\}$, then we have

$$M_i = \sum_j \lambda_j^{(i)} \Lambda_j^{(i)},$$

where $\lambda_j^{(i)}$ indicates the measurement result assigned to $\Lambda_j^{(i)}$. Since there are multiple ways to write an operator as a weighted sum of measurements, we define $Z_{\mathcal{M}}(\mathcal{O})$, the "$\mathcal{M}$-DFE scale factor", to be the minimal Z over all possible ways of writing $\mathcal{O}$ as a weighted sum of measurements in $\mathcal{M}$. This is formally defined as the following:

$$\begin{aligned} Z_{\mathcal{M}}(\mathcal{O}) &= \min_{\{M_i\} \subseteq \mathcal{M}} Z(\mathcal{O}) \\ &= \min_{\substack{\{M_i\} \subseteq \mathcal{M}, \{f_i\}, C \\ \text{s.t.} \sum_i f_i M_i = \mathcal{O} - CI}} \sum_i \left(\lambda_{\max}^{(i)} - \lambda_{\min}^{(i)} \right) |f_i|, \end{aligned} \tag{4.10}$$

where $\lambda_{\max}^{(i)}$ and $\lambda_{\min}^{(i)}$ indicate the maximum and minimum of measurement result assignments of the POVM $\left\{\Lambda_j^{(i)}\right\}$ for achieving M_i. $Z(\mathcal{O})$ satisfies nonnegativity, homogeneity, and the triangle inequality, and hence can be interpreted as a norm. Note that when perfect projection to the state is available, i.e. $|\psi\rangle\langle\psi| \in \mathcal{M}$, we have $Z_{\mathcal{M}}(|\psi\rangle\langle\psi|) = 1$ because M can be chosen to be $|\psi\rangle\langle\psi|$. Here, the POVM is $\{|\psi\rangle\langle\psi|, I - |\psi\rangle\langle\psi|\}$. There are also situations where assigning different ranges for different measurements would improve the variance and hence the overall performance, but for simplicity, we only consider fixed ranges in the main text. The analysis for general POVMs and unbounded measurements is in Appendix A.1. As mentioned above, if the set of measurements is linearly independent, Z can be evaluated as the 1-norm, but for linearly dependent sets, it and the corresponding probability distribution have to be evaluated by solving a linear program, yet the dimension of the variables is often infinite, making the evaluation difficult in practice. This difficulty is reflected by the

conjectured entries in the tables.

So far we have considered performing generalized DFE of arbitrary operators and characterized the efficiency. Next, we utilize this method to perform DFE-based tomography in a subspace and identify cases where such tomography can be done efficiently.

Definition 2. Define a state space $\mathcal{S}$ to have a cost of β with $\mathcal{M}$ if and only if the following two conditions are satisfied.

$$\dim \mathcal{S} \leq \beta, \tag{4.11}$$

$$\max_{\substack{|\psi\rangle \in \mathcal{S} \\ \langle\psi|\psi\rangle = 1}} Z_{\mathcal{M}}(|\psi\rangle\langle\psi|) \leq \beta. \tag{4.12}$$

Lemma 2. *A* $\mathrm{poly}(m)$ *dimensional space* $\mathcal{S}$ *has a* $\mathrm{poly}(m)$ *cost with* $\mathcal{M}$ *if and only if there exists an orthonormal basis* $\{|\psi_a\rangle\}$ *such that*

$$\max_{1 \leq a,b \leq \dim \mathcal{S}, c \in \{0,1\}} Z_{\mathcal{M}}(i^c |\psi_a\rangle\langle\psi_b| + h.c.) = O\left(\mathrm{poly}(m)\right).$$

Lemma 3. *Given a* $\mathrm{poly}(m)$*-cost space* $\mathcal{S}$ *with* $\mathcal{M}$*,* $\rho_{\mathcal{S}} = P_{\mathcal{S}} \rho P_{\mathcal{S}}$ *can be determined with probability* $1 - \delta$ *within Frobenius distance* ϵ *by performing* $\mathrm{poly}(m, \ln \delta, \epsilon^{-1})$ *measurements from* $\mathcal{M}$*.*

The proofs of lemmas are in Appendix A.2. Lemma 2 and 3 establish that the capability of performing efficient DFE of any state in a polynomial subspace guarantees efficient tomography of the projected density operator. For neighborhood subspaces, under certain conditions, one only needs to be capable of performing DFE of a base state $|\psi\rangle$ efficiently, because it guarantees that any states within the neighborhood subspace generated from this state will also have efficient DFE by expanding the measurements to include Hadamard tests with the generators of the neighborhood (see Fig. 4.1). To state this efficiency condition of neighborhood subspace formally:

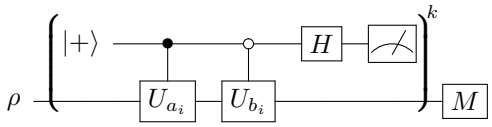

Figure 4.1: An example of a measurement in the Hadamard-expanded set of measurements $\mathcal{M}$, generated by performing multiple Hadamard tests with $U \in \mathcal{U}$, followed by the measurement $M \in \mathcal{M}'$. This allows efficient estimation of $\mathrm{tr}\left(U_a^\dagger |\psi\rangle\langle\psi| U_b\right)$.

Theorem 1. *Given a basis state $|\psi\rangle$ and a base set of measurements $\mathcal{M}'$, if $\mathcal{M}'$ permits efficient DFE of $|\psi\rangle$, i.e.*

$$Z_{\mathcal{M}'}\left(|\psi\rangle\langle\psi|\right) = O(\mathrm{poly}(m)),$$

then for $N_k(|\psi\rangle, \mathcal{U})$, the neighborhood generated from $|\psi\rangle$ by up to k applications of unitaries from $\mathcal{U}$, define the Hadamard-test-expanded set of measurements $\mathcal{M}$ to be

$$\mathcal{M} := \left\{\mathcal{C}(M) \mid M \in \mathcal{M}', \mathcal{C} \in \mathbb{O}\right\},$$

where $\mathbb{O}$ is the set of all sequences of controlled unitaries from $\mathcal{U}$ with ancilla qubits as control preceded by preparing such ancilla in $|+\rangle$ states followed by measuring these ancillae (See FIG. 4.1). If $k = O(1)$, $|\mathcal{U}| = O(\mathrm{poly}(m))$, then

$$Z_{\mathcal{M}}\left(i^c \prod_{i=1}^{k} U_{a_i} |\psi\rangle\langle\psi| \left(\prod_{j=1}^{k} U_{b_j}\right)^\dagger + h.c.\right) = O(\mathrm{poly}(m)),$$

where $U_{a_i}, U_{b_i} \in \{I\} \cup \mathcal{U}$.

Furthermore, consider the Gram matrix $G_{\vec{a}\vec{b}} = \langle\psi| \left(\prod_{i=1}^{k} U_{a_i}\right)^\dagger \prod_{j=1}^{k} U_{b_j} |\psi\rangle$ of the neighborhood basis $\left\{\prod_{j=1}^{k} U_{a_j} |\psi\rangle\right\}$, then

$$\max_{\substack{|\psi'\rangle \in N_k(|\psi\rangle, \mathcal{U}) \\ \langle\psi'|\psi'\rangle = 1}} Z_{\mathcal{M}}(|\psi'\rangle\langle\psi'|) = O\left(\mathrm{poly}(m, \|G^+\|_2)\right).$$

Here, G^+ is the Moore–Penrose inverse of G. In other words, $\|G^+\|_2$ is the inverse of the smallest nonzero eigenvalue of G. Therefore, if $\|G^+\|_2 = O(\mathrm{poly}\,(m))$, then the DFE cost of any state in the neighborhood is $O(\mathrm{poly}\,(m))$.

The proof of Theorem 1 is deferred to the Appendix A.2. In most physically relevant cases, $\|G^+\|_2 = O(1)$. In particular, if $\{\prod_{i=1}^{k} U_{a_i}|\psi\rangle\}$ is an orthonormal set, G is the identity matrix, and hence $\|G^+\|_2 = 1$. In this theorem, the crucial condition for the set of measurements to be sufficient for efficient DFE within the neighborhood subspace is that the measurement set is invariant under the Hadamard test. Most sets of measurements are invariant under Hadamard tests of local unitaries. For example, a product measurement preceded by any number of Hadamard tests of single qubit unitaries is still a product measurement. Thus, with these assumptions, any neighborhood around any DFE-efficient state generated by local operators allows for efficient DFE-based tomography. For example, if the set of possible measurements is the set of all product measurements, since local operations do not alter the product property of operators, the set of product measurements is invariant under local Hadamard tests. For Pauli measurements, although the Pauli group is not closed under arbitrary local operation, any local operation can only transform a single qubit Pauli operator into an operator with a 2-norm of at most 1, effectively rotating the axis of measurements. In the worst case, the new axis direction would be equidistant from the three principle axes, introducing a factor of $\sqrt{3}$ to the DFE cost. Hence, up to a constant k, such efficiency is still retained. The expansion of measurements with Hadamard tests can also be viewed as a method to expand the available set of POVM with controlled unitaries, for example, Pauli measurements are expanded to product measurements with local Hadamard tests, and product measurements in turn can be expanded to quasilocal measurements with Hadamard tests of two-qubit gates.

Finally, we present our DEMESST algorithm to perform tomography of a polynomial subspace as in Algorithm 1. The resultant operator is an unbiased estimator of the projected

Algorithm 1: DEMESST. The inputs are the basis $\{|\psi_j\rangle\}$, the available set of measurements $\mathcal{M}$, and the sample count for the elements t_{jl}, while the output is an estimate of ρ in the basis provided, i.e. $\rho_{jl} \sim \langle\psi_j\,|\,\rho\,|\,\psi_l\rangle$. For $j = l$, t_{jj} indicates the sample count for the diagonal element ρ_{jj}. For $j < l$, t_{jl} indicates the sample count for the real part of ρ_{jl}, while t_{lj} indicates the sample count for the imaginary part.

Data: $\{|\psi_j\rangle\}, \mathcal{M}, t_{jl}$
Result: $\rho_{jl} \sim \langle\psi_j\,|\,\rho\,|\,\psi_l\rangle$
$\rho \leftarrow$ Zeros($|\{|\psi_j\rangle\}|, |\{|\psi_j\rangle\}|$);
for $j \leftarrow 1$ *to* $|\{|\psi_j\rangle\}|$ **do**
  Find C and f_i such that $|\psi_j\rangle\langle\psi_j| = C + \sum_i f_i M_i$;
  for $a \leftarrow 1$ *to* t_{jj} **do**
    Randomly sample and measure M_i with $p_i = \frac{|f_i|}{\sum_i |f_i|}$, and assign the measurement result to X_a;
  end
  $\rho_{jj} \leftarrow$ Average of $sgn(f_{i_a}) X_a$;
  for $l \leftarrow j+1$ *to* $|\{|\psi_j\rangle\}|$ **do**
    Find C and f_i such that $|\psi_j\rangle\langle\psi_l| + h.c. = C + \sum_i f_i M_i$;
    for $a \leftarrow 1$ *to* t_{jl} **do**
      Randomly sample and measure M_i with $p_i = \frac{|f_i|}{\sum_i |f_i|}$ and assign the measurement result to X_a;
    end
    $\rho_{jl} \leftarrow$ Average of $\frac{1}{2} sgn(f_{i_a}) X_a$;
    Find C and f_i such that $i|\psi_j\rangle\langle\psi_l| + h.c. = C + \sum_i f_i M_i$;
    for $a \leftarrow 1$ *to* t_{lj} **do**
      Randomly sample and measure M_i with $p_i = \frac{|f_i|}{\sum_i |f_i|}$ and assign the measurement result to X_a;
    end
    $\rho_{lj} \leftarrow \rho_{jl} -$ Average of $\frac{i}{2} sgn(f_{i_a}) X_a$;
    $\rho_{jl} \leftarrow \rho_{jl} +$ Average of $\frac{i}{2} sgn(f_{i_a}) X_a$;
  end
end

density operator, and is not guaranteed to be positive semidefinite nor trace 1. In particular, the expected value of the trace is equal to the trace of the product of the physical state and the projection to the subspace. Hence, this procedure can self-verify: if the trace is close to one, the physical state is indeed mostly in such a subspace; if the state is mostly outside of the subspace, it will be reflected through the trace. If the application requires a positive semidefinite operator, one can project to the nearest physical state [55].

4.5 DFE Cost: Examples

With this framework, we analyze classes of states with efficient DFE and the corresponding sets of operators that can generate poly(m)-cost subspaces.

4.5.1 Pauli Measurements and Stabilizer States

Firstly, we revisit the classical example of stabilizer states:

Corollary 2. *If $|\psi\rangle$ is a stabilizer state, tomography of the neighborhood space generated with polynomially many different Pauli operators, i.e. $N_k(|\psi\rangle,\mathcal{U})$, where $\mathcal{U} \subseteq \mathcal{P}$, $|\mathcal{U}| = O(\text{poly}(m))$, and $k = O(1)$, can be done with a polynomial number of Pauli measurements.*

The Pauli DFE cost factor of any Hermitian operator is

$$Z_{\mathcal{P}}(\mathcal{O}) = 2^{1-m} \sum_{P \in \{I,\sigma_x,\sigma_y,\sigma_z\}^{\otimes m}} |\text{tr}\left(P\widetilde{\mathcal{O}}\right)|. \tag{4.13}$$

For a stabilizer state, this would be $2^{1-m}(2^m - 1) = 2 - 2^{1-m}$, since within 2^m stabilizers, only $2^m - 1$ are nontrivial. The neighborhood basis (or its subset, since if the product of two Paulis is proportional to a stabilizer, the two states will be identical up to a global phase) is orthonormal, hence the Gram matrix will have a bounded $\|G^+\|_2$. Therefore, from Theorem

1, one can perform efficient tomography of the neighborhood subspace with Hadamard-expanded Pauli measurements. However, to prove the corollary, we need to go further and show that Pauli measurements are sufficient to perform the tomography efficiently. Hence, we consider the elements of the neighborhood basis directly. The off-diagonal elements in the neighborhood basis,

$$(P_i|\psi\rangle)(\langle\psi|P_j^\dagger) = 2^{-m}\sum_{s\in S} P_i s P_j^\dagger, \tag{4.14}$$

is also an average of Pauli operators. After separating Hermitian and anti-Hermitian parts, we can sample it similarly to DFE of the stabilizer state, with $Z_{\mathcal{P}} \leq 2 - 2^{1-m}$; therefore, the DFE of any element in the neighborhood basis and hence the tomography is efficient. Furthermore, since this process has no requirements beyond the stabilizer formalism, the generating Pauli operators can be non-local, such as single-qubit errors propagating through a Clifford circuit. Any Pauli error in a Clifford circuit would end up as a (potentially different) Pauli error in the final state. Hence, if we prepare a stabilizer state from a product state through a Clifford circuit with $\mathfrak{m}$ single or two-qubit gates, we can cover up to k gate errors by considering the neighborhood generated by up to k applications of the $\leq 15\mathfrak{m}$ possible Pauli gate errors (15 corresponds to the number of nontrivial Paulis for two qubits), which has $O((15\mathfrak{m})^k)$ possibilities. This can be further extended to process tomography of circuits with $O(\ln \mathfrak{m})$ non-Clifford gates by representing non-Clifford gates as superpositions of Paulis and performing DFE of the Choi operator [56]. Note that to perform DFE of the Choi operator, we do not need to physically prepare maximally entangled states with ancilla qubits. Instead, we can prepare product stabilizer states and measure the output state according to the Pauli operator being sampled on the Choi state. This is listed as the first column in TABLE 4.1.

4.5.2 Wigner Measurements and GKP states

Continuous variable systems have states analogous to stabilizer states in multiqubit systems, i.e. GKP states [57], the eigenstates of certain commuting sets of displacement operators. For example, $|\psi\rangle = \left(\sum_{s=-\infty}^{\infty} |q = \sqrt{2\pi}s\rangle\right)^{\otimes m}$ is an m-mode square lattice GKP state. Such states are stabilized by displacement operators D_α and displaced parity operators $D_\alpha(-1)^{\sum \hat{n}} D_\alpha^\dagger$, as long as the displacement $\vec{\alpha}$ is a lattice vector of the state. Similar to qubit stabilizer states, DFE of such states also have a constant overhead with a simple set of measurements:

Corollary 3. *If $|\psi\rangle\langle\psi|$ is an ideal GKP state and $\mathcal{M}$ consists of all Wigner measurements, i.e. $\langle M(\vec{\alpha})\rangle_\rho = \langle D_\alpha(-1)^{\sum \hat{n}} D_\alpha^\dagger\rangle_\rho = \left(\frac{\pi}{2}\right)^m W_\rho(\vec{\alpha})$, the DFE cost of $|\psi\rangle\langle\psi|$ is 2.*

The overlap of two operators can be written as the overlap of the Wigner functions:

$$\begin{aligned} \mathrm{tr}(\rho\sigma) &= \pi^m \int d^{2m}\vec{\alpha}\; W_\rho(\vec{\alpha}) W_\sigma(\vec{\alpha}) \\ &= 2^m \int d^{2m}\vec{\alpha}\; \left(\left(\frac{\pi}{2}\right)^m W_\rho(\vec{\alpha})\right) W_\sigma(\vec{\alpha}), \end{aligned} \tag{4.15}$$

and the associated cost factor satisfies:

$$Z_{\mathcal{W}}(\sigma) = 2^{m+1} \int d^{2m}\vec{\alpha}\; |W_\sigma(\vec{\alpha})|. \tag{4.16}$$

The Wigner function of a GKP state can only take values of 0 or $\pm\left(\frac{2}{\pi}\right)^m$, therefore

$$\begin{aligned} Z_{\mathcal{W}}(|\psi\rangle\langle\psi|) &= 2^{m+1} \int d^{2m}\vec{\alpha}\; |W_\psi(\vec{\alpha})| \\ &= 2\pi^m \int d^{2m}\vec{\alpha}\; \left(W_\psi(\vec{\alpha})\right)^2 \\ &= 2. \end{aligned} \tag{4.17}$$

Equivalently, we are sampling each lattice point with equal probability. This is listed as the

first column in TABLE 4.2.

4.5.3 Product Measurements and Product States

Pauli and Wigner measurements can attain small overheads for some states, such as the examples above. However, there exist simple states that have exponential DFE costs with such measurements.

For example, DFE of the tensor product of m magic states

$$|\psi\rangle\langle\psi| = \left(\frac{I + 3^{-1/2}\left(\sigma_x + \sigma_y + \sigma_z\right)}{2}\right)^{\otimes m}, \tag{4.18}$$

with Pauli measurements has an associated cost factor $Z_{\mathcal{P}}$ that scales exponentially as the mode number grows:

$$Z_{\mathcal{P}}(|\psi\rangle\langle\psi|) = 2^{1-m}\left(\left(1+\sqrt{3}\right)^m - 1\right) = \Theta\left(\left(\frac{1+\sqrt{3}}{2}\right)^m\right). \tag{4.19}$$

However, if we have access to arbitrary product measurements, including projection to arbitrary product states, this would allow for sampling the fidelity directly, and hence $Z = 1$ if $\mathcal{M}$ is the set of all product measurements.

A simple example in multimode bosonic system that has an exponential DFE tomography cost with Wigner measurement is the multimode vacuum state, i.e.

$$|\psi\rangle\langle\psi| = |0\rangle\langle 0|^{\otimes m}. \tag{4.20}$$

Since $Z_{\mathcal{W}}(\mathcal{O}) = 2^{m+1}\int d^{2m}\vec{\alpha}|W_{\widetilde{\mathcal{O}}}(\vec{\alpha})|$,

$$Z_{\mathcal{W}}(|\psi\rangle\langle\psi|) = 2^{m+1}\int d^{2m}\vec{\alpha}\left(\frac{2}{\pi}\right)^m e^{-2|\vec{\alpha}|^2} = 2^{m+1}. \tag{4.21}$$

However, if Husimi Q function measurements are allowed, including the product of projection to the vacuum of individual modes, the Q function at the origin will sample the fidelity, hence $Z_{\mathcal{Q}} = 1$. Note that to perform neighborhood tomography around coherent states, a combination of Q and W measurements are often needed to effectively perform the Hadamard tests. This combination is the protocol used by He et al. [6]. However, the cost of DFE tomography of any normalizable state with only Wigner measurements Z_W, including any finite energy GKP states, scales exponentially with the number of modes since

$$Z_{\mathcal{W}}(|\phi\rangle\langle\phi|) = 2^{m+1} \int d^{2m}\vec{\alpha} |W_\phi(\vec{\alpha})| \tag{4.22}$$

$$\leq 2^{m+1} \left| \int d^{2m}\vec{\alpha} W_\phi(\vec{\alpha}) \right| = 2^{m+1}. \tag{4.23}$$

Therefore, a spanning set of product measurements is not always efficient, although the set of arbitrary product measurements is sufficient for performing efficient DFE of arbitrary product states:

Corollary 4. *If $|\psi\rangle$ is a product state, tomography of the neighborhood space generated with local operators $\mathcal{K}_{local}$, i.e. $N_k(|\psi\rangle, \mathcal{K}_{local})$, where $|\mathcal{K}_{local}| = O(\text{poly}(m))$ and $k = O(1)$, can be done in a polynomial number of product measurements.*

There exists an orthonormal basis of the neighborhood subspace where every basis state is a product state, and any $|\psi_a\rangle\langle\psi_b|$ is a projection to a single party pure state in at least $m-2k$ parties. Since only maximally $2k$ modes involve nontrivial measurements, $Z = 2^{O(k)} = O(1)$. For example, our method is demonstrated experimentally to be effective in a multimode bosonic system on the subspace of maximally one photon among up to five modes [6]. This corresponds to $N_1(|0\rangle^{\otimes m}, \{\hat{a}_i^\dagger\})$, which is $m+1$ dimensional. Off-diagonal terms are of the form of $|0\rangle\langle 0|^{\otimes m-1} \otimes |1\rangle\langle 0|$ or $|0\rangle\langle 0|^{\otimes m-2} \otimes |1\rangle\langle 0| \otimes |0\rangle\langle 1|$, which were estimated by projecting $|0\rangle\langle 0|$ modes to vacuum and performing Wigner tomography in the remaining modes. This is listed as the second column in TABLE 4.1 & the third column in TABLE 4.2.

4.5.4 Quasilocal Measurements and Matrix Product States

With some multimode controls, one can extend the set of DFE-efficient states further to include MPS:

Corollary 5. *If arbitrary quasilocal unitaries (i.e. arbitrary gates between any two subsystems) and single qubit measurements are allowed, tomography of any polynomial subspace spanned by MPSs with a fixed maximal bond dimension $k = O(1)$ can be performed efficiently with $O(1)$ ancilla qubits and $O(m)$ arbitrary two-qubit gates per measurement.*

This follows from [58], which showed that any MPS state with bond dimension k can be efficiently converted to a product state with quasilocal unitaries, namely arbitrary unitaries between any specified qubit and a k-dimensional ancilla system. Hence, the quasilocal-DFE scale factor of MPS with a small bond dimension is 1. Since the superposition of two MPS states of bond dimension k can be written as a MPS state of bond dimension $2k$, we can perform DFE of it efficiently with $1+\lceil \log_2 k \rceil$ ancilla qubits and arbitrary $(2+\lceil \log_2 k \rceil)$-qubit unitaries. In particular,

$$\mathcal{M} = \left\{ \left[\left(\prod_{i=1}^{m} U_i \right)^{\dagger} M \left(\prod_{i=1}^{m} U_i \right) \right] \middle| M \in \mathcal{M}_{prod}, \right. \\ \left. U_i \text{ is a unitary between } i^{th} \text{ qubit and the ancillas} \right\}. \tag{4.24}$$

Here $\mathcal{M}_{prod}$ indicates the set of product measurements. From that, we can extract the off-diagonal components and construct the projected density operator efficiently. This is listed as the third column in TABLE 4.1. Compared to MPS tomography [25, 26], our scheme is limited to predetermined reference states, but allows fidelity estimation even when the infidelity is large. In particular, even when the physical state requires intractably large bond dimensional MPO to describe, our scheme can still be used to determine the fidelity with the reference states.

4.5.5 Gaussian Unitaries and Gaussian States

Similarly, with arbitrary Gaussian unitaries, any pure Gaussian state in a multimode bosonic system can be efficiently converted to a vacuum state. Hence, we have the following, which is listed as the fourth column in TABLE 4.2:

Corollary 6. *If arbitrary Gaussian unitaries and single-mode measurements are allowed, DFE of arbitrary pure Gaussian states is efficient.*

DEMESST can be extended to multiple base states, as long as DFE of any superposition of the base states can be performed efficiently. The base state condition is not bounded by limited entanglement: it only requires DFE of any superposition of the base states, which can be done efficiently if the base states are well-structured, as demonstrated by the example of stabilizer states. The relevant space would then be the combination of the individual neighborhoods of the base states.

4.6 Discussion and Conclusion

Our DEMESST framework has additional important features. First, DEMESST can *self-verify* the polynomial neighborhood subspace assumption and, similarly, can determine the projected state even if a major part of the physical state is outside of the subspace. Second, DEMESST can work with a large class of states that can be highly entangled, as long as the DFE cost factor is tractable, without requiring any structure of the states. Furthermore, Generalized DFE can also be used to accommodate methods to determine some nonlinear properties of a density operator with joint measurement on multiple copies of the state. For example, determining purity $\mathrm{tr}(\rho^2)$ with joint Bell measurements of two copies of multiqubit states can be interpreted as performing the DFE of the SWAP operator with two copies of ρ as the state to be sampled, since $\mathrm{tr}(\rho^2) = \mathrm{tr}(\mathrm{SWAP}\rho \otimes \rho)$.

In conclusion, we have presented a generalized version of DFE to minimize variance and

shown an error bound for it. We have described DEMESST, a partial tomography of the neighborhood of a multipartite pure state with polynomial sampling complexity. Future directions include proving or disproving efficient DFE of an arbitrary pure state with LOCC measurements, which would allow DEMESST of any polynomial subspace with a polynomial number of measurements (refer to Appendix A.3), demonstrating or disproving a superpolynomial lower bound of cost for MPS, Gaussian states, and arbitrary pure states with more complicated measurements (refer to TABLES 4.1 & 4.2), which, if disproven, may expand the set of possible DFE-efficient states as base states we can use in practice. Other directions include finding algorithm to determine Z with product measurements efficiently, and adopt techniques from other tomography methods to more efficiently obtain the projected density matrix with DFE as oracle. Note that if the physical measurements are not limited within the subspace, techniques like Maximal Likelihood Estimation are expected to require DFE as oracle to utilize the polynomial subspace projection, and would perform poorly without it, as terms outside the subspace would affect the individual measurement results.

CHAPTER 5

LOCAL UNITARY DECOMPOSITION OF TRIPARTITE ARBITRARY LEVELED QUDIT STABILIZER STATES INTO p-LEVEL-QUDIT EPR AND GHZ STATES

5.1 Introduction

Various quantum protocols have been proposed based on distributed quantum architectures. Quantum protocols, such as quantum key distribution, distributed quantum sensing, and distributed quantum computing, rely on efficient entanglement distribution across multiple nodes. Understanding and manipulating multipartite entangled states is thus critical for shaping entanglement into desired forms, such as GHZ or EPR states, for these applications. While general tripartite pure states are equivalent to bipartite mixed states and lack a full characterization beyond density matrices, specific classes like stabilizer states admit simpler descriptions. Bravyi et al. [59] showed that tripartite qubit stabilizer states are reducible via local Clifford unitaries to GHZ states, EPR pairs, and unentangled qubits, a result extended by Looi et al. [60] to squarefree qudit dimensions. Unlike prior work limited to squarefree D, analyzing $D = p^n$ involves handling states requiring more than N generators, where N is the number of qudits. Since theorem 4 of [60] establishes an isomorphism between stabilizer formalism with composite non-prime-power D and a tensor product of prime-power $D_i' = p_i^{n_i}$ stabilizer formalisms, where $\prod_i D_i' = D$, in this chapter we consider $D = p^n$, and the results extend to arbitrary D due to the isomorphism. In this chapter, we refer to generalized Pauli and generalized Clifford as Pauli and Clifford for simplicity.

Using a novel tool, subsystem phase matrix, to capture entanglement properties, we extend these results to arbitrary qudit dimensions D, including prime-power cases, by allowing local unitaries beyond the Clifford group. Section 5.2 discusses special properties of prime-power stabilizer states, Section 5.3 defines the subsystem phase matrix, Section 5.4 presents

key lemmas, and Section 5.5 details our main decomposition theorems.

5.2 Special Properties of Prime Power Dimension Stabilizer States

Recall from Sec. 2.3 that stabilizer states with nonsquarefree D can have a stabilizer group with higher dimension than the number of qudits. Such phenomena is not limited to a single qudit. One remarkable example is the $D = 9$ $N = 3$ state stabilized by $S = \langle X_1X_2X_3, X_1^3X_2^6, Z_1Z_2Z_3, Z_1^3Z_2^6\rangle$ is not connected to the GHZ state, stabilized by $S' = \langle X_1X_2X_3, Z_1Z_2^8, Z_1Z_3^8\rangle$, through any Clifford operation, yet they are connected by some qudit-local unitaries. The two states can be written as products of two $D = 3$ GHZ states in different ways:

$$\begin{aligned}|S\rangle = &\frac{1}{3}\left(|000\rangle + |012\rangle + |021\rangle + |102\rangle + |111\rangle + |120\rangle + |201\rangle + |210\rangle + |222\rangle\right) \\ &\otimes \frac{1}{\sqrt{3}}\left(|000\rangle + |111\rangle + |222\rangle\right),\end{aligned} \tag{5.1}$$

$$|S\rangle' = \frac{1}{\sqrt{3}}\left(|000\rangle + |111\rangle + |222\rangle\right) \otimes \frac{1}{\sqrt{3}}\left(|000\rangle + |111\rangle + |222\rangle\right). \tag{5.2}$$

However, due to the structure of the prime-power-dimensional qudit Pauli group, one cannot rotate the first part without affecting the second part with $D = 9$ Clifford unitaries, since Clifford unitaries cannot alter the dimension of a subgroup of the Pauli group. As demonstrated by this state, analysis based only on Clifford operations cannot thoroughly analyze the entanglement properties of stabilizer states with prime power D. To accommodate such states, we introduce a tool that is invariant under arbitrary local Clifford operations and simultaneously allow some local unitaries beyond Clifford group.

5.3 Definition of Subsystem Phase Matrix

Most entanglement characterization of stabilizer states with squarefree D relies on having the same number of generators as the number of qudits, which is generally invalid for prime power D. To characterize local Clifford invariants in such situation, we define subsystem phase matrices, which capture the commutation relations of stabilizers across parties.

Definition 3 (Subsystem Phase Matrix)**.** A set of m $\left(\mathbb{Z}_{p^n}\right)^{\mathcal{N}\times\mathcal{N}}$ matrices $\{M_\alpha\}$ is a valid set of subsystem phase matrices for an m-partite $D = p^n$ stabilizer state $|S\rangle$ if and only if there exists a pair of functions $f : S \to \left(\mathbb{Z}_{p^n}\right)^{\mathcal{N}}$ and $F : \left(\mathbb{Z}_{p^n}\right)^{\mathcal{N}} \to S$ such that

$$\forall s, s' \in S, s_\alpha s'_\alpha = \omega^{f^T(s')M_\alpha f(s)} s'_\alpha s_\alpha, \tag{5.3}$$

$$\forall v, v' \in \left(\mathbb{Z}_{p^n}\right)^{\mathcal{N}}, F(v)_\alpha F(v')_\alpha = \omega^{v'^T M_\alpha v} F(v')_\alpha F(v)_\alpha, \tag{5.4}$$

where $\mathcal{N}$ is an integer and $\{\alpha\} = \{1, 2, \ldots, m\}$ is the set of subsystems. Note that for any product operator $\hat{O}$, we represent its part in subsystem α as $\hat{O}_\alpha$, such that $\prod_\alpha \hat{O}_\alpha = \hat{O}$. Equivalently, given a generating set of stabilizers $\left\{g^{(i)}\right\}$, a valid set of subsystem phase matrices $\left\{M_{\alpha,ij}\right\}$ can be obtained through the module representation of the generators:

$$M_{\alpha,ij} = r^{(i)^T} \Omega_\alpha r^{(j)} \tag{5.5}$$

where $r^{(i)}$ is the module element corresponding to the stabilizer $g^{(i)}$, i.e. $\sigma_{r^{(i)}} \propto g^{(i)}$, and Ω_α is the bilinear form restricted to only subsystem α. In terms of operators, this corresponds to

$$g_\alpha^{(j)} g_\alpha^{(i)} = \omega^{M_{\alpha,ij}} g_\alpha^{(i)} g_\alpha^{(j)}. \tag{5.6}$$

Note that these matrices are antisymmetric because $\Omega_\alpha = -\Omega_\alpha^T$, and the sum of phase

matrices over all subsystems gives 0, since all stabilizers commute, i.e.

$$M_{\alpha,ii} = 0, M_\alpha + M_\alpha^T = 0, \sum_\alpha M_\alpha = 0. \tag{5.7}$$

It is trivial to see that such matrices are invariant under local Clifford unitaries, and any two stabilizer states that are equivalent up to some local Clifford unitaries must have the same matrices up to some basis transform. These subsystem phase matrices contain all entanglement information of tripartite stabilizer states, which will be proven in a subsequent section. In the simplified case of a pure bipartite stabilizer state, diagonalizing such matrices identifies pairs of generators that are non-commuting in subsystems, revealing the extractable entangled qudit pairs.

Such matrices are also invariant under some local non-Clifford unitaries. For example, if a stabilizer state $|\psi\rangle$ has $Z_1^{p^{n-1}}$ as a stabilizer, the following non-Clifford unitary

$$V_1 = \frac{1}{\sqrt{p}} \sum_{j=0}^{p^{n-1}-1} \sum_{k=0}^{p-1} \sum_{l=0}^{p-1} \omega^{p^{n-1}kl} |p^{n-1}k + j\rangle\langle pj + l|_1 \tag{5.8}$$

can transform the state into another stabilizer state without altering the subsystem phase matrix. If we decompose the $D = p^n$ qudit into n $D = p$ qudits with $p-$nary representation, this unitary corresponds to applying Hadamard gate on the lowest qudit and then moving it to the highest. We can see that $V_1^\dagger Z_1^p V_1 |\psi\rangle = Z_1|\psi\rangle$ and $V_1^\dagger X_1 V_1 |\psi\rangle = X_1^p |\psi\rangle$, thus V_1 scales up Z_1 and scales down X_1, resulting in a new stabilizer state with $X_1^{p^{n-1}}$ as an extra stabilizer generator. The subsystem phase matrix is unaltered because the scaling cancels out. In the following sections, we also use the projection of the subsystem phase matrix into the subring $\mathbb{Z}_p$, M'_a, which is defined as

$$M'_{a,ij} = M_{a,ij} \bmod p. \tag{5.9}$$

5.4 Important Lemmas

Lemma 4. *Given a stabilizer group S that specifies a unique D-level qudit pure stabilizer state, any Pauli operator g that commutes with all stabilizers must be a stabilizer up to some phase, i.e.*

$$|S| = D^N, \forall s \in S, [g, s] = 0 \Rightarrow \exists \phi \ s.t. \ \omega^\phi g \in S, \tag{5.10}$$

where ϕ is an integer for odd D and integer/half-integer for even D.

Proof.

$$g|S\rangle\langle S|g^\dagger = g\left(D^{-N/2}\sum_{s\in S} s\right)g^\dagger = D^{-N/2}\sum_{s\in S} gsg^\dagger = D^{-N/2}\sum_{s\in S} s = |S\rangle\langle S|. \tag{5.11}$$

Therefore, $g|S\rangle \propto |S\rangle$ and $|\langle S \,|\, g \,|\, S\rangle| = 1$. To show that ϕ must be an integer/half-integer, consider

$$\langle S \,|\, g \,|\, S\rangle = \mathrm{tr}\,(g|S\rangle\langle S|) = D^{-N}\sum_{s\in S} \mathrm{tr}\, gs^\dagger. \tag{5.12}$$

Since both g and s are elements of the Pauli group, $\mathrm{tr}\, gs^\dagger = 0$ if $g \not\propto s$ and $\mathrm{tr}\, gs^\dagger = D^N\omega^\phi$ if $g = \omega^\phi s$. Because there must not be two elements that differ only by a phase in a stabilizer group, there must be one and only one s that is proportional to g, and $gs^\dagger$ is proportional to identity. Since ϕ is an integer/half-integer if and only if $\omega^\phi I$ is a Pauli, it must be true. □

Lemma 5. *If a $D = p^n$ pure stabilizer state is stabilized by $\prod_{r\in R} X_r$ and pairwise $Z_r^{p^{n-n'}} Z_{r'}^{-p^{n-n'}}$ over some number of qudits R, where $|R| \geq 2$ and $1 \leq n' \leq n$, then there is some local unitary operation that extracts a $D' = p^{n'}$ $|R|$-qudit GHZ/EPR state.*

$$\begin{aligned} &X_r^{\otimes_{r\in R}} \in S, \forall r, r' \in R, Z_r^{p^{n-n'}} Z_{r'}^{-p^{n-n'}} \in S \\ &\Rightarrow \exists \{U_r\} \ \ s.t. \ \left(\bigotimes_{r\in R} U_r\right)\left(|S\rangle \otimes |0\rangle_p^{\otimes r\in R}\right) = |\tilde{S}\rangle \otimes |GHZ\rangle_{p^{n'}}, \end{aligned} \tag{5.13}$$

where

$$\tilde{S} = \bar{S} \otimes \left\langle Z_{r_1}^{p^{n-n'}} \right\rangle, \tag{5.14}$$

$$\bar{S} = \left\{ s \in S \middle| \left[s, Z_r^{p^{n-n'}} \right] = 0 \right\}, \tag{5.15}$$

$$|GHZ\rangle_{p^{n'}} = p^{-n'/2} \sum_{k=0}^{p^{n'}-1} |k\rangle_r^{\otimes r \in R}. \tag{5.16}$$

Note that if $|R| = 2$, the extracted state is an EPR pair, otherwise it is a GHZ state.

Proof. Write the state as a summation over the lowest n' sub-p-it of the $|R|$ involved qudits in the p-nary representation

$$|S\rangle = \sum_{\vec{v}} w_{\vec{v}} |\varphi_{\vec{v}}\rangle \otimes |\vec{v}\rangle. \tag{5.17}$$

For the state to be stabilized by the pairwise $Z_r^{p^{n-n'}} Z_{r'}^{-p^{n-n'}}$, only terms with $\vec{v} \propto \vec{1}$ can be nonzero, where $\vec{1} = (1, 1, \ldots, 1)^T$ is the $|R|$-dimensional vector/module element of all 1s, i.e.

$$|S\rangle = \sum_{j=0}^{p^{n'}-1} w_{j\vec{1}} |\varphi_{j\vec{1}}\rangle \otimes |j\vec{1}\rangle, \tag{5.18}$$

where $j\vec{1} = (j, j, \ldots, j)^T$. $\prod_{r \in R} X_r$ further limits all weights and state with different j to be same, i.e.

$$|S\rangle = \sum_{j=0}^{p^{n'}-1} w_{\vec{0}} |\varphi_{\vec{0}}\rangle \otimes |j\vec{1}\rangle, \tag{5.19}$$

where $\vec{0} = (0, 0, \ldots, 0)^T$. Hence,

$$|S\rangle = |\varphi_{\vec{0}}\rangle \otimes |GHZ\rangle_p. \tag{5.20}$$

It is clear that every stabilizer can be split into two parts: one operating on $|\varphi\rangle$ and one

operating on the GHZ/EPR state. In other words,

$$S = \bar{S} \otimes \left\{ \prod_{r \in R} X_r^j \;\middle|\; 0 \leq j \leq p^{n'} - 1 \right\}. \tag{5.21}$$

Note that $\bar{S}$ includes $\prod_{r \in R} X_r^{p^{n'}}$ and $Z_r^{p^{n-n'}} Z_{r'}^{-p^{n-n'}}$. Swapping the GHZ/EPR state with $|0\rangle_{p^{n'}}^{\otimes r \in R}$ gives $|\varphi_{\vec{0}}\rangle \otimes |0\rangle_{p^{n'}}^{\otimes r \in R}$, and it is trivial to show that this state is stabilized by $\tilde{S}$. □

Note that we added $|0\rangle_p^{n'}$ states to effectively store GHZ/EPR states, but in principle the procedure can be done in place by performing analysis of Pauli groups of a mixture of $D = p, p^2, \ldots, p^n$ qudits using symplectic modules [61], and update the definition of Pauli group and Clifford group between every step.

5.5 Main results

We present the main corollary, stating that all $D = p^n$ tripartite pure stabilizer states can be reduced to $D = p$ GHZ states, EPR pairs, and unentangled qudits with local unitaries, followed by the two theorems that enables the corollary. These theorems hold generally for m-partite stabilizer states, with $m = 3$ corresponding to the tripartite case.

Corollary 7. *There exist some local unitaries that convert a tripartite pure $D = p^n$ stabilizer state into a tensor product of GHZ states, EPR pairs, and unentagled qudits over p-level systems.*

$$\begin{aligned} &\exists U_a \in \mathbb{U}_a, U_b \in \mathbb{U}_b, U_c \in \mathbb{U}_c \text{ s.t. } U_a \otimes U_b \otimes U_c |S\rangle \\ &= |GHZ\rangle_p^{\otimes N_{GHZ}} \otimes |EPR\rangle_{p,ab}^{\otimes N_{ab}} \otimes |EPR\rangle_{p,ac}^{\otimes N_{ac}} \otimes |EPR\rangle_{p,bc}^{\otimes N_{bc}} \otimes |0\rangle_{p,a}^{\otimes N_a} \otimes |0\rangle_{p,b}^{\otimes N_b} \otimes |0\rangle_{p,c}^{\otimes N_c}. \end{aligned}$$

Proof. The subsystem phase matrices of any tripartite pure $D = p^n$ stabilizer state must satisfy at least one of the following conditions:

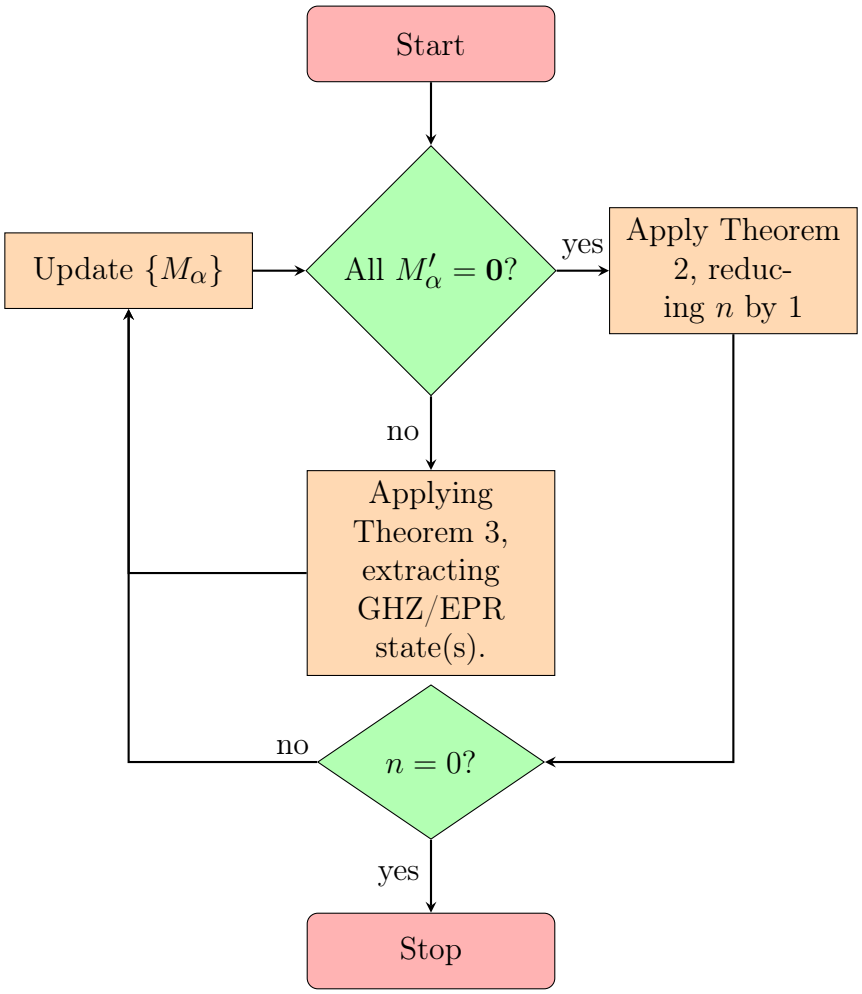

Figure 5.1: Flowchart of entanglement extraction

1. All projected subsystem phase matrices are trivial.

$$\forall \alpha, M'_\alpha = \mathbf{0} \tag{5.22}$$

2. The intersection of the spans of all subsystem phase matrices is nontrivial.

$$\bigcap_\alpha \text{span}(M_\alpha) \neq \{\mathbf{0}\} \tag{5.23}$$

3. There exists at least one $\vec{v}$ such that $\vec{v}$ is in the span of two subsystem phase matrices and $p^{n-1}\vec{v}$ is not in the span of the remaining subsystem phase matrix.

$$\exists \alpha, \vec{v} \text{ s.t. } \vec{v} \in \bigcap_{\beta \neq \alpha} \text{span}(M_\beta), p^{n-1}\vec{v} \notin \text{span}(M_\alpha) \tag{5.24}$$

These conditions correspond to Theorem 2, Corollary 8, and Corollary 9 respectively. Theorem 2 allows reduction of n by 1, while Corollary 8 and 9, implications of Theorem 3, allow extraction of entanglement in the form of $D = p$ GHZ/EPR state(s). We can then follow the entanglement extraction flowchart shown in Fig. 5.1 to iteratively reduce n while extracting GHZ/EPR state(s).

To show that at least one of the conditions must hold, consider the situation where conditions 1 and 2 are false, i.e. at least one projected subsystem phase matrix is nontrivial, and the intersection of all subsystem phase matrices is trivial. Without loss of generality, assume $M'_a \neq \mathbf{0}$, let $\vec{\bar{v}}$ be a nonzero column of M'_a, and $\vec{v}$ be the corresponding column of M_a. Since $\vec{\bar{v}}$ is a nontrivial element, $\vec{v}$ must be of order p^n. Since $p^{n-1}\vec{v} \in \text{span}(M_a)$, condition 2 being false implies that $p^{n-1}\vec{v}$ must be absent from at least one of span (M_b) or span (M_c), without loss of generality assume $p^{n-1}\vec{v} \notin$ span (M_c). Then, there exists invertible $\mathcal{N} \times \mathcal{N}$

matrix L such that

$$L\vec{v} = \left(\begin{array}{c} 1 \\ \hline 0 \\ \vec{0} \end{array}\right), \tag{5.25a}$$

$$LM_cL^T = \left(\begin{array}{c|cc} 0 & 0 & \vec{0}^T \\ \hline 0 & \multicolumn{2}{c}{\multirow{2}{*}{$\widetilde{M}_c$}} \\ \vec{0} & & \end{array}\right). \tag{5.25b}$$

$$LM_aL^T = \left(\begin{array}{c|cc} 0 & 1 & \vec{0}^T \\ \hline -1 & \multicolumn{2}{c}{\multirow{2}{*}{$\widetilde{M}_a$}} \\ \vec{0} & & \end{array}\right), \tag{5.25c}$$

$$LM_bL^T = \left(\begin{array}{c|cc} 0 & -1 & \vec{0}^T \\ \hline 1 & \multicolumn{2}{c}{\multirow{2}{*}{$-\widetilde{M}_a - \widetilde{M}_c$}} \\ \vec{0} & & \end{array}\right). \tag{5.25d}$$

We justify the existence of L in the following four steps: (1) For a vector $\vec{v}$ of order p^n, there exists a matrix $L^{(1)}$ that satisfies Eq. 5.25a. (2) Since $p^{n-1}\vec{v} \notin \text{span}(M_c)$, we can eliminate the entries in the first row and first column of M_c to obtain $L^{(2)}$ that satisfies Eq. 5.25b by applying similarity transformations over rows and columns, while preserving the structure of Eq. 5.25a. (3) Because $\vec{v} \in \text{span}(M_a)$, the first row and first column of M_a remain order p^n after the above transformation. By performing additional similarity transformations, we can obtain $L^{(3)}$ that satisfies Eq. 5.25c, while maintaining the structure of Eqs. 5.25a and 5.25b. (4) Finally, we obtain Eq. 5.25d using Eq. 5.7.

According to Eqs. 5.25c and 5.25d, we have $\vec{v}' = L^{-1}\left(\begin{array}{c} 0 \\ \hline 1 \\ \vec{0} \end{array}\right)$ is in the span of both M_a and M_b. Due to $p^{n-1}\vec{v}' \in M_a \cap M_b$, condition 2 being false implies $p^{n-1}\vec{v}' \notin M_c$,

thus $\vec{v}'$ must satisfy condition 3. Therefore, for any $n \geq 1$, the subsystem phase matrices must satisfy at least one condition. By iteratively applying the theorems according to the flowchart in Fig. 5.1, any tripartite stabilizer state can be decomposed into p-level GHZ states, EPR pairs, and unentangled qudits. Since entanglement cannot be infinite for a state with finite qudits, eventually we will reach a product state, i.e. $M_a = M_b = M_c = 0$, with $n = 1$, which we can rotate all qudits to $|0\rangle_p$. Ancillary qudits introduced in Theorem 3 are not required to extract the entanglement but simplifies the process. Note that although the unitaries involved are always Cliffords for some power of p, the combination is generally not a $D = p^n$ Clifford unitary. □

Theorem 2. *If $\forall\alpha, M'_\alpha = 0$, then the m-partite stabilizer state is local-Clifford equivalent to a product of a $D' = p^{n-1}$ stabilizer state and unentangled $D'' = p$ qudits.*

$$\forall\alpha, M_\alpha \equiv 0 \,(\mathrm{mod}\ p) \Rightarrow \exists U_\alpha \in \mathbb{C}_\alpha \ s.t. \ \left(\bigotimes_\alpha U_\alpha\right)|S\rangle = |\tilde{S}'\rangle_{p^{n-1}} \otimes |0\rangle_p^{\otimes N}. \tag{5.26}$$

Proof. Since $M'_\alpha = 0$, projecting the stabilizer group into $D = p$ Pauli group results in a stabilizer group where every pair of stabilizer commutes in every subsystem, and hence there exists a set of local $D = p$ Clifford unitaries that transform the projected stabilizer group to consist of only products of Zs. Hence, there exists some local $D = p^n$ Clifford that transforms the original stabilizer group to consist of only products of Zs and X^ps. In the resultant stabilizer state, $Z^{p^{n-1}}$ of every single qudit commutes with all stabilizers, and thus, from Lemma 4, is a stabilizer up to some phase, which can be removed by applying Xs. As the state is now stabilized by $Z^{p^{n-1}}$ of individual qudits, if we write the computational basis in p-nary representation, the lowest p-dit is 0 for every qudit, i.e.

$$\bigotimes_\alpha U_\alpha|S\rangle = |\tilde{S}\rangle = |\psi\rangle_{p^{n-1}} \otimes |0\rangle^{\otimes N}. \tag{5.27}$$

To show that $|\psi\rangle_{p^{n-1}}$ is a stabilizer state, consider

$$X^p|\tilde{S}\rangle = \left(X'|\psi\rangle_{p^{n-1}}\right) \otimes |0\rangle^{\otimes N}, \tag{5.28}$$

$$Z|\tilde{S}\rangle = \left(Z'|\psi\rangle_{p^{n-1}}\right) \otimes |0\rangle^{\otimes N}, \tag{5.29}$$

and since $\tilde{S}$ consists of only products of Zs and X^ps, replacing X^p with X results in a $D = p^{n-1}$ stabilizer group. □

Theorem 3. *For a pure $D = p^n$ stabilizer state, if there exists an order-p^n module element $\vec{v}$ such that $p^{n-n'}\vec{v}$ is in the span of m' subsystem phase matrices, where $1 \leq n' \leq n$, and $p^{n-1}\vec{v}$ is not in the span of the sum of the m' subsystem phase matrices, then we can extract n' copies of m'-partite $D = p$ GHZ/EPR state. Note that if $m' = 2$, the extracted state(s) is/are EPR pairs.*

$$\exists \mathfrak{B} \subseteq \{\alpha\}, \vec{v} \text{ s.t. } \vec{v} \not\equiv \vec{0} \,(\mathrm{mod} p)\,, p^{n-n'}\vec{v} \in \bigcap_{\beta\in\mathfrak{B}} \mathrm{span}\left(M_\beta\right), p^{n-1}\vec{v} \notin \mathrm{span}\left(\sum_\beta M_\beta\right)$$
$$\Rightarrow \exists U_\beta \in \mathbb{U}_\beta \text{ s.t. } \left(\bigotimes_{\beta\in\mathfrak{B}} U_\beta\right)|S\rangle \otimes |0\rangle_{p^{n'},\mathfrak{B}} = |\tilde{S}\rangle \otimes |GHZ\rangle_{p,\mathfrak{B}}^{\otimes n'}. \tag{5.30}$$

Proof. Since $p^{n-1}\vec{v} \notin \mathrm{span}\left(\sum_{\beta\in\mathfrak{B}} M_\beta\right)$ and $\sum_{\beta\in\mathfrak{B}} M_\beta$ are antisymmetric, there exists $\vec{v}' \in \ker\left(\sum_{\beta\in\mathfrak{B}} M_\beta\right)$ such that $\vec{v}'^T\vec{v} = 1$. There also exists $\vec{u}^{(\beta)}$ such that $M_\beta\vec{u}^{(\beta)} = p^{n-n'}\vec{v}$. We now have

$$\left(\sum_{\beta\in\mathfrak{B}} M_\beta\right)\vec{v}' = \vec{0}, \tag{5.31}$$

$$\vec{v}'^T M_\beta \vec{u}^{(\beta)} = p^{n-n'}, \tag{5.32}$$

$$p^{n'} M_\beta \vec{u}^{(\beta)} = 0. \tag{5.33}$$

Denote the stabilizers corresponding to $\vec{v}'$ and $\vec{u}^{(\beta)}$ as g and $h^{(\beta)}$ respectively, and let k_β

be the minimal integer satisfying $h_\beta^{(\beta)^{p^{k_\beta}}} \propto I$. Then, there exists local Clifford that rotates $h_\beta^{(\beta)}$ to

$$h_\beta'^{(\beta)} \propto Z_{\beta,1}^{p^{n-k_\beta}}. \tag{5.34}$$

where $Z_{\beta,1}$ indicates a clock operator on the first qubit of the subsystem β. If $k_\beta > n'$, then Eq. 5.33 indicates $Z_{\beta,1}^{p^{n-k_\beta+n'}}$ commutes with all stabilizers, and hence is a stabilizer up to some phase. Apply suitable $X_{\beta,1}$ to erase the phase, then we can apply $V_{\beta,1}$ $k_\beta - n'$ times, resulting in

$$h_\beta''^{(\beta)} \propto Z_{\beta,1}^{p^{n-n'}}. \tag{5.35}$$

Now we have $Z_{\beta,1}^{p^{n-n'}} g' = \omega^{p^{n-n'}} g' Z_{\beta,1}^{p^{n-n'}}$, so there exists local Clifford that conserves all $h_\beta'^{(\beta)}$ and rotates g' to

$$g'' = \bigotimes_{\beta\in\mathfrak{B}} X_{\beta,1} \otimes \bigotimes_{\alpha\notin\mathfrak{B}} g_\alpha. \tag{5.36}$$

From Lemma 4, Eq. 5.31 indicates that now $\bigotimes_{\beta\in\mathfrak{B}} X_{\beta,1}$ is a stabilizer up to some phase, while $M_\beta \vec{u}^{(\beta)} - M_{\beta'} \vec{u}^{(\beta')} = 0$ indicates that $Z_{\beta,1}^{p^{n-n'}} Z_{\beta',1}^{-p^{n-n'}}$ is also a stabilizer up to some phase. After erasing the phases by applying suitable Xs and Zs, we can extract an m'-partite $D = p^{n'}$ GHZ/EPR state using Lemma 5, which is equivalent to n' copies of $D = p$ GHZ/EPR states. □

Based on Theorem 3, we can take special values for n' and $\mathfrak{B}$ to obtain the following two corollaries:

Corollary 8. *For a triparite pure $D = p^n$ stabilizer state, if the intersection of the spans of all subsystem phase matrices is nontrivial, then GHZ state(s) can be extracted.*

Proof. Let $\vec{v}$ be a nontrivial element of $\bigcap_\alpha \mathrm{span}(M_\alpha)$ and its order be $p^{n'}$, then there exists an order-p^n $\vec{v}$ such that $p^{n-n'}\vec{v} = \vec{v}$. This satisfies the conditions of Theorem 3 with $\mathfrak{B} = \{a, b, c\}$, hence n' copies of GHZ state(s) can be extracted. □

Corollary 9. *For a tripartite pure $D = p^n$ stabilizer state, if there exists at least one $\vec{v}$ such that $\vec{v}$ is in the span of two subsystem phase matrices and $p^{n-1}\vec{v}$ is not in the span of the remaining subsystem phase matrix, then n copies of EPR pair(s) can be extracted.*

Proof. Since $p^{n-1}\vec{v}$ not within the span of a matrix implies that $\vec{v}$ is of order p^n, this satisfies the conditions of Theorem 3 with $\mathfrak{B}$ being the two relevant subsystems and $n' = n$, hence n copies of EPR pair(s) can be extracted. □

5.6 Conclusion

We generalize the decomposition of tripartite stabilizer states to arbitrary qudit dimensions, enabling entanglement manipulation for prime-power systems previously inaccessible with Clifford operations. This facilitates protocols such as entanglement shaping [62] and quantum secret sharing in arbitrary-level qudit systems. Future work could explore applying this method to more subsystems, the possibility of characterizing any m-partite stabilizer state with subsystem phase matrices and/or reducing all $D = p^n$ stabilizer states to $D = p$ stabilizer states with local unitaries beyond Clifford operations.

CHAPTER 6

OUTLOOK

This dissertation presents several schemes utilizing local operations for distribution, certification, and manipulation of quantum entanglement. In particular, Chapter 2 describes how a second pass assists photon capture for a cavity with tunable coupling; Chapter 3 demonstrates how measurements capability affects complexity scaling in state certification; and Chapter 4 depicts how local unitaries decompose tripartite stabilizer states of qubits with p^n levels into EPR pairs and GHZ states. These schemes illustrate how local capabilities commonly considered as "sufficiently complete", i.e. single pass of tunable coupling for photon capture, Pauli or Wigner measurements for state tomography, and Clifford unitaries for stabilizer state transformation, could be inefficient for certain tasks and can be improved with minor additions.

In addition to discussion and collection sections in previous chapters, here are some caveats and outlook on future directions of the covered schemes:

- In the two-pass photon capture scheme, the coupling is assumed to be point-like, the cavity is assumed to be single-mode, and the whole process is assumed to be linear. Without such assumptions, especially linearity, the outcome of the process is no longer fully described by one scale parameter, and other complications such as thermal noise and non-Markovian dynamics would only further complicate the process. Therefore, application of this scheme on a physical device would require optimization beyond the simplified model described in the scheme. Therefore, a realistic model factoring in realistic limitations can facilitate implementation of the scheme in experiments.

- In the DFE subspace tomography scheme, the separations established are only applicable when no assumptions can be made. For example, with the assumption of no correlated error, Lee et. al. [63] recently showed that the fidelity of the preparation of

certain non-stabilizer states, such as $|T\rangle$, can be estimated using Pauli measurements efficiently by twirled purity estimation. Gupta et. al. [64] recently showed LOCC measurements can certify arbitrary n-qubit states efficiently up to a factor of n in infidelity, but it is currently unknown whether they suffice to efficiently estimate fidelity for arbitrary pure states.

- In the decomposition of tripartite stabilizer states, the gates involved, the Clifford gates of $p^{n'}$-level qudits with n' ranging from 1 to n, would form a universal set for any $n \geq 2$. In particular, Clifford unitaries of $D = 2$ and $D = 4$ could generate the qubit T gate when combined. Therefore, in general, implementing the gates required with high fidelity could be difficult and thus the use of this scheme would be limited to entanglement characterization. The extendibility towards more party is also unclear as there are unlimited indecomposible stabilizer states with only local unitaries when there are more than three subsystems, as shown by Englbrecht et.al.[65], even for qubits. Therefore, the current approach of identifying extractable $D = p$ states would not extend directly. It is also unknown whether all multipartite $D = p^n$ stabilizer states could be converted into $D = p$ stabilizer states with local unitary, and whether LOCC could provide more reversible conversions between stabilizers states in the multipartite context.

REFERENCES

[1] E. T. Khabiboulline, J. Borregaard, K. De Greve, and M. D. Lukin, Optical interferometry with quantum networks, Phys. Rev. Lett. **123**, 070504 (2019).

[2] A. Broadbent, Delegating private quantum computations, Canadian Journal of Physics **93**, 941–946 (2015).

[3] Y. Wong and L. Jiang, Recycling reflections for perfect photon capture, Phys. Rev. A **112**, 032412 (2025).

[4] H. K. Warner, J. Holzgrafe, B. Yankelevich, D. Barton, S. Poletto, C. Xin, N. Sinclair, D. Zhu, E. Sete, B. Langley, *et al.*, Coherent control of a superconducting qubit using light, Nature Physics , 1–8 (2025).

[5] Y. Wong, M. Yuan, K. He, S. Chakram, A. Seif, D. I. Schuster, and L. Jiang, Efficient quantum tomography of a polynomial subspace (2025), arXiv:2503.00255 [quant-ph] .

[6] K. He, M. Yuan, Y. Wong, S. Chakram, A. Seif, L. Jiang, and D. I. Schuster, Efficient multimode wigner tomography, Nature Communications **15**, 4138 (2024).

[7] Y. Wong and L. Jiang, Local unitary decomposition of tripartite arbitrary leveled qudit stabilizer states into p-level-qudit epr and ghz state (2025), arXiv:2507.09416 [quant-ph] .

[8] C. Oh, S. Chen, Y. Wong, S. Zhou, H.-Y. Huang, J. A. H. Nielsen, Z.-H. Liu, J. S. Neergaard-Nielsen, U. L. Andersen, L. Jiang, and J. Preskill, Entanglement-enabled advantage for learning a bosonic random displacement channel, Phys. Rev. Lett. **133**, 230604 (2024).

[9] Z.-H. Liu, R. Brunel, E. E. Østergaard, O. Cordero, S. Chen, Y. Wong, J. A. Nielsen, A. B. Bregnsbo, S. Zhou, H.-Y. Huang, *et al.*, Quantum learning advantage on a scalable photonic platform, Science **389**, 1332–1335 (2025).

[10] Y. Huang, X. Ren, B. Li, Y. Wong, Z. Liang, and L. Jiang, Peer-to-peer distribution of graph states across spacetime quantum networks of arbitrary topology, Proc. ACM Meas. Anal. Comput. Syst. **9**, 10.1145/3727123 (2025).

[11] S.-u. Lee, C. Oh, Y. Wong, S. Chen, and L. Jiang, Universal spreading of conditional mutual information in noisy random circuits, Phys. Rev. Lett. **133**, 200402 (2024).

[12] B. Li, Z. Wang, G. Zheng, Y. Wong, and L. Jiang, Optimality condition for the petz map, Phys. Rev. Lett. **134**, 200602 (2025).

[13] C. Oh, Y. Lim, Y. Wong, B. Fefferman, and L. Jiang, Quantum-inspired classical algorithms for molecular vibronic spectra, Nature Physics **20**, 225–231 (2024).

[14] Z. Wang, M. Zhang, Y. Wong, C. Zhong, and L. Jiang, Optimized protocols for duplex quantum transduction, Phys. Rev. Lett. **131**, 220802 (2023).

[15] C. Oh, S. Zhou, Y. Wong, and L. Jiang, Quantum limits of superresolution in a noisy environment, Phys. Rev. Lett. **126**, 120502 (2021).

[16] W.-L. Ma, M. Zhang, Y. Wong, K. Noh, S. Rosenblum, P. Reinhold, R. J. Schoelkopf, and L. Jiang, Path-independent quantum gates with noisy ancilla, Phys. Rev. Lett. **125**, 110503 (2020).

[17] C. W. Gardiner and M. J. Collett, Input and output in damped quantum systems: Quantum stochastic differential equations and the master equation, Phys. Rev. A **31**, 3761–3774 (1985).

[18] V. Gebhart, R. Santagati, A. A. Gentile, E. M. Gauger, D. Craig, N. Ares, L. Banchi, F. Marquardt, L. Pezze, and C. Bonato, Learning quantum systems, Nature Reviews Physics **5**, 141–156 (2023).

[19] Z. Hradil, Quantum-state estimation, Phys. Rev. A **55**, R1561–R1564 (1997).

[20] R. Blume-Kohout, Optimal, reliable estimation of quantum states, New Journal of Physics **12**, 043034 (2010).

[21] C. Ferrie, Self-guided quantum tomography, Physical Review Letters **113**, 10.1103/physrevlett.113.190404 (2014).

[22] J. Haah, A. W. Harrow, Z. Ji, X. Wu, and N. Yu, Sample-optimal tomography of quantum states, IEEE Transactions on Information Theory , 1–1 (2017).

[23] D. Gross, Y.-K. Liu, S. T. Flammia, S. Becker, and J. Eisert, Quantum State Tomography via Compressed Sensing, Physical Review Letters **105**, 150401 (2010).

[24] G. Tóth, W. Wieczorek, D. Gross, R. Krischek, C. Schwemmer, and H. Weinfurter, Permutationally invariant quantum tomography, Phys. Rev. Lett. **105**, 250403 (2010).

[25] M. Cramer, M. B. Plenio, S. T. Flammia, R. Somma, D. Gross, S. D. Bartlett, O. Landon-Cardinal, D. Poulin, and Y.-K. Liu, Efficient quantum state tomography, Nature Communications **1**, 149 (2010).

[26] B. P. Lanyon, C. Maier, M. Holzäpfel, T. Baumgratz, C. Hempel, P. Jurcevic, I. Dhand, A. S. Buyskikh, A. J. Daley, M. Cramer, M. B. Plenio, R. Blatt, and C. F. Roos, Efficient tomography of a quantum many-body system, Nature Physics **13**, 1158–1162 (2017).

[27] T. Baumgratz, D. Gross, M. Cramer, and M. B. Plenio, Scalable Reconstruction of Density Matrices, Physical Review Letters **111**, 020401 (2013).

[28] G. Carleo and M. Troyer, Solving the quantum many-body problem with artificial neural networks, Science **355**, 602–606 (2017), https://www.science.org/doi/pdf/10.1126/science.aag2302 .

[29] S. Aaronson, Shadow tomography of quantum states, SIAM Journal on Computing **49**, STOC18–368–STOC18–394 (2020), https://doi.org/10.1137/18M120275X .

[30] H.-Y. Huang, R. Kueng, and J. Preskill, Predicting many properties of a quantum system from very few measurements, Nature Physics **16**, 1050–1057 (2020).

[31] S. T. Flammia and Y.-K. Liu, Direct Fidelity Estimation from Few Pauli Measurements, Physical Review Letters **106**, 230501 (2011).

[32] M. P. da Silva, O. Landon-Cardinal, and D. Poulin, Practical Characterization of Quantum Devices without Tomography, Physical Review Letters **107**, 210404 (2011).

[33] H. J. Kimble, The quantum internet, Nature **453**, 1023–1030 (2008).

[34] N. Lauk, N. Sinclair, S. Barzanjeh, J. P. Covey, M. Saffman, M. Spiropulu, and C. Simon, Perspectives on quantum transduction, Quantum Science and Technology **5**, 020501 (2020).

[35] J. I. Cirac, P. Zoller, H. J. Kimble, and H. Mabuchi, Quantum state transfer and entanglement distribution among distant nodes in a quantum network, Physical Review Letters **78**, 3221–3224 (1997).

[36] D. N. Matsukevich and A. Kuzmich, Quantum state transfer between matter and light, Science **306**, 663–666 (2004).

[37] A. D. Boozer, A. Boca, R. Miller, T. E. Northup, and H. J. Kimble, Reversible state transfer between light and a single trapped atom, Physical Review Letters **98**, 193601–193604 (2007).

[38] A. Stute, B. Casabone, B. Brandstätter, K. Friebe, T. E. Northup, and R. Blatt, Quantum-state transfer from an ion to a photon, Nature Photonics **7**, 219–222 (2013).

[39] C. J. Axline, L. D. Burkhart, W. Pfaff, M. Zhang, K. Chou, P. Campagne-Ibarcq, P. Reinhold, L. Frunzio, S. M. Girvin, L. Jiang, M. H. Devoret, and R. J. Schoelkopf, On-demand quantum state transfer and entanglement between remote microwave cavity memories, Nature Physics **14**, 705–710 (2018).

[40] M. Stobińska, G. Alber, and G. Leuchs, Perfect excitation of a matter qubit by a single photon in free space, Europhysics Letters **86**, 14007 (2009).

[41] H. Yan, Y. Zhong, H.-S. Chang, A. Bienfait, M.-H. Chou, C. R. Conner, E. Dumur, J. Grebel, R. G. Povey, and A. N. Cleland, Entanglement purification and protection in a superconducting quantum network, Physical Review Letters **128**, 10.1103/physrevlett.128.080504 (2022).

[42] S. Ritter, C. Nölleke, C. Hahn, A. Reiserer, A. Neuzner, M. Uphoff, M. Mücke, E. Figueroa, J. Bochmann, and G. Rempe, An elementary quantum network of single atoms in optical cavities, Nature **484**, 195–200 (2012).

[43] S. T. Flammia, D. Gross, Y.-K. Liu, and J. Eisert, Quantum tomography via compressed sensing: error bounds, sample complexity and efficient estimators, New Journal of Physics **14**, 095022 (2012).

[44] T. Baumgratz, A. Nüßeler, M. Cramer, and M. B. Plenio, A scalable maximum likelihood method for quantum state tomography, New Journal of Physics **15**, 125004 (2013).

[45] F. Huszár and N. M. T. Houlsby, Adaptive Bayesian quantum tomography, Physical Review A **85**, 052120 (2012).

[46] Y. Quek, S. Fort, and H. K. Ng, Adaptive quantum state tomography with neural networks, npj Quantum Information **7**, 1–7 (2021).

[47] G. Torlai, G. Mazzola, J. Carrasquilla, M. Troyer, R. Melko, and G. Carleo, Neural-network quantum state tomography, Nature Physics **14**, 447–450 (2018).

[48] E. S. Tiunov, V. V. Tiunova (Vyborova), A. E. Ulanov, A. I. Lvovsky, and A. K. Fedorov, Experimental quantum homodyne tomography via machine learning, Optica **7**, 448–454 (2020).

[49] J. Barberà-Rodríguez, M. Navarro, and L. Zambrano, Sampling groups of pauli operators to enhance direct fidelity estimation, Quantum **9**, 1784 (2025).

[50] O. Fawzi, A. Oufkir, and R. Salzmann, Optimal fidelity estimation from binary measurements for discrete and continuous variable systems, PRX Quantum , – (2025).

[51] N. Guo, F. Pan, and P. Rebentrost, Estimating properties of a quantum state by importance-sampled operator shadows (2024), arXiv:2305.09374 [quant-ph] .

[52] V. V. Albert, S. O. Mundhada, A. Grimm, S. Touzard, M. H. Devoret, and L. Jiang, Pair-cat codes: autonomous error-correction with low-order nonlinearity, Quantum Science and Technology **4**, 035007 (2019).

[53] S. Chakram, K. He, A. V. Dixit, A. E. Oriani, R. K. Naik, N. Leung, H. Kwon, W.-L. Ma, L. Jiang, and D. I. Schuster, Multimode photon blockade, Nature Physics **18**, 879–884 (2022).

[54] M. Yuan, A. Seif, A. Lingenfelter, D. I. Schuster, A. A. Clerk, and L. Jiang, Universal control in bosonic systems with weak kerr nonlinearities, Phys. Rev. A **111**, 032606 (2025).

[55] J. A. Smolin, J. M. Gambetta, and G. Smith, Efficient method for computing the maximum-likelihood quantum state from measurements with additive gaussian noise, Phys. Rev. Lett. **108**, 070502 (2012).

[56] E. Bäumer, V. Tripathi, D. S. Wang, P. Rall, E. H. Chen, S. Majumder, A. Seif, and Z. K. Minev, Efficient long-range entanglement using dynamic circuits, PRX Quantum **5**, 030339 (2024).

[57] D. Gottesman, A. Kitaev, and J. Preskill, Encoding a qubit in an oscillator, Phys. Rev. A **64**, 012310 (2001).

[58] C. Schön, K. Hammerer, M. M. Wolf, J. I. Cirac, and E. Solano, Sequential generation of matrix-product states in cavity qed, Phys. Rev. A **75**, 032311 (2007).

[59] S. Bravyi, D. Fattal, and D. Gottesman, Ghz extraction yield for multipartite stabilizer states, Journal of Mathematical Physics **47**, 10.1063/1.2203431 (2006).

[60] S. Y. Looi and R. B. Griffiths, Tripartite entanglement in qudit stabilizer states and application in quantum error correction, Physical Review A **84**, 10.1103/physreva.84.052306 (2011).

[61] J.-P. Tignol and S. A. Amitsur, Symplectic modules, Israel Journal of Mathematics **54**, 266–290 (1986).

[62] C. Zhong, Y. Wong, and L. Jiang, Entanglement trimming in stabilizer formalism (2021), arXiv:2103.09932 [quant-ph] .

[63] S. un Lee, M. Yuan, S. Chen, K. Tsubouchi, and L. Jiang, Efficient benchmarking of logical magic state (2025), arXiv:2505.09687 [quant-ph] .

[64] M. Gupta, W. He, and R. O'Donnell, Few single-qubit measurements suffice to certify any quantum state (2025), arXiv:2506.11355 [quant-ph] .

[65] M. Englbrecht, T. Kraft, and B. Kraus, Transformations of Stabilizer States in Quantum Networks, Quantum **6**, 846 (2022).

[66] M. J. Wainwright, *High-Dimensional Statistics: A Non-Asymptotic Viewpoint*, Cambridge Series in Statistical and Probabilistic Mathematics (Cambridge University Press, 2019).

APPENDIX A

SUPPLEMENTARY MATERIALS FOR SECTION 4.4

A.1 DFE cost with POVM / unbounded measurements

In general, one can obtain a Hoeffding's bound with POVM and unbound assigned values as long as the distribution of the measurement result is subgaussian for any physical state. The condition for a distribution of measurements to be subgaussian is to have a finite subgaussian norm [66], which is defined as follows for quantum measurements:

$$\|X\|_{\psi_2} = \inf_{c>0} \max_{\substack{\rho \\ s.t.\sum_{i,j} p_i \operatorname{tr}(\rho\Lambda_j^{(i)}) e^{\left(\lambda_j^{(i)}\right)^2/c^2} \leq 2}} c, \tag{A.1}$$

where X is the random variable representing the measurement result, $\{\Lambda_j^{(i)}\}$ is the i^{th} POVM, p_i is the probability of choosing i^{th} POVM, and $\lambda_j^{(i)}$ is the measurement result assigned to $\Lambda_j^{(i)}$. We can minimize over all possible distributions that realize an operator $\mathcal{O}$:

$$\|\mathcal{O}\|_{\psi_2,\mathcal{L}} = \min_{\substack{\{\Lambda_j^{(i)}\}\in\mathcal{L},\{\lambda_j^{(i)}\},\{p_i\},C \\ s.t.\sum_{i,j} p_i\lambda_j^{(i)}\Lambda_j^{(i)} = \mathcal{O} - CI}} \|X\|_{\psi_2}, \tag{A.2}$$

where $\mathcal{L}$ is the set of available POVMs. For any $\mathcal{O}$ with finite $Z_{\mathcal{M}}(\mathcal{O})$, we have $Z_{\mathcal{M}}(\mathcal{O}) \geq \|\mathcal{O}\|_{\psi_2,\mathcal{L}}/\sqrt{\ln 2}$, since any bounded random variable is also subgaussian. Conversely, with any finite $\|\mathcal{O}\|_{\psi_2,\mathcal{L}}$, we have a Hoeffding bound of

$$\delta_t = \mathbb{P}_t\left(\left|\frac{1}{t}\sum_{j=1}^{t} X_j + C - \langle\mathcal{O}\rangle_\rho\right| \geq \epsilon\right) \leq 2e^{-\Omega(t\epsilon^2\|\mathcal{O}\|_{\psi_2,\mathcal{L}}^{-2})}. \tag{A.3}$$

Hence, $\|\mathcal{O}\|_{\psi_2,\mathcal{L}}$ is a generalized version of the DFE cost.

A.2 Proofs of lemmas and theorem 1

A.2.1 Lemma 2

Proof. Proof for the 'only if' statement:

$$\begin{aligned} & i^c|\psi_a\rangle\langle\psi_b| + h.c. \\ =& 2 \cdot \frac{1}{2}\left(|\psi_a\rangle + i^{-c}|\psi_b\rangle\right)\left(\langle\psi_a| + i^c\langle\psi_b|\right) \\ & - |\psi_a\rangle\langle\psi_a| - |\psi_b\rangle\langle\psi_b|, \end{aligned} \tag{A.4}$$

$$\begin{aligned} & Z_{\mathcal{M}}(i^c|\psi_a\rangle\langle\psi_b| + h.c.) \\ \leq& 2Z_{\mathcal{M}}\left(\frac{1}{2}\left(|\psi_a\rangle + i^{-c}|\psi_b\rangle\right)\left(\langle\psi_a| + i^c\langle\psi_b|\right)\right) \\ & + Z_{\mathcal{M}}(|\psi_a\rangle\langle\psi_a|) + Z_{\mathcal{M}}(|\psi_b\rangle\langle\psi_b|) \\ =& O(\text{poly}(m)). \end{aligned} \tag{A.5}$$

Proof for the 'if' statement:

$$\begin{aligned} & Z_{\mathcal{M}}\left(\sum_a \alpha_a|\psi_a\rangle \sum_b \alpha_b^*\langle\psi_b|\right) \\ \leq& \sum_{a>b}\Big(Z_{\mathcal{M}}\left(|\psi_a\rangle\langle\psi_b| + h.c.\right)|\text{Re}(\alpha_a\alpha_b^*)| \\ & + Z_{\mathcal{M}}\left(i|\psi_a\rangle\langle\psi_b| + h.c.\right)|\text{Im}(\alpha_a\alpha_b^*)|\Big) \\ & + \sum_a Z_{\mathcal{M}}(|\psi_a\rangle\langle\psi_a|)|\alpha_a|^2 \\ =& O(\text{poly}(m)). \end{aligned} \tag{A.6}$$

□

A.2.2 Lemma 3

Proof. Each $i^c|\psi_a\rangle\langle\psi_b| + i^{-c}|\psi_b\rangle\langle\psi_a|$ can be determined to ϵ' precision with $1-\delta'$ probability with $t = \frac{Z^2}{2\epsilon'^2}\ln\frac{2}{\delta'} = O\left(\text{poly}(m, \ln\delta', \epsilon'^{-1})\right)$ measurements. Hence, setting $\delta' = \delta/(\dim\mathcal{S})^2$ and $\epsilon' = \epsilon/\dim\mathcal{S}$, we can determine $\rho_\mathcal{S}$ with $(\dim\mathcal{S})^2 t = O\left(\text{poly}(m, \ln\delta, \epsilon^{-1})\right)$ measurements. □

A.2.3 Theorem 1

Proof. The diagonal elements of the density matrix on the neighborhood basis can be estimated by rotating the basis state to the base state followed by DFE of the base state. To estimate the off-diagonal elements, we apply controlled unitaries on the subsystems with differing unitaries on both sides, and the required elements can be calculated through the difference in the results. For example, the real part of $\langle U_a^\dagger \mathcal{O} U_b\rangle$ can be calculated by performing a Hadamard test on controlled unitaries U_a and U_b:

$$\begin{aligned}\text{Re}\left(\langle U_a^\dagger \mathcal{O} U_b\rangle\right) = \frac{1}{2}\Bigg(&\left\langle\left(\frac{U_a+U_b}{\sqrt{2}}\right)^\dagger \mathcal{O}\left(\frac{U_a+U_b}{\sqrt{2}}\right)\right\rangle \\ &- \left\langle\left(\frac{U_a-U_b}{\sqrt{2}}\right)^\dagger \mathcal{O}\left(\frac{U_a-U_b}{\sqrt{2}}\right)\right\rangle\Bigg).\end{aligned} \tag{A.7}$$

By performing up to $2k$ Hadamard tests, followed by the original measurement, we can perform DFE for operators within the neighborhood of any DFE-efficient state.

Any pure state within the neighborhood can be written as a superposition of $\prod_{i=1}^k U_{a_i}|\psi\rangle$ with coefficients $\leq \|G^+\|_2$, hence $Z_\mathcal{M} = O(\text{poly}(m, \|G^+\|_2))$. □

A.3 LOCC Conjecture

To systematically generate a DFE of any arbitrary pure state with only LOCC measurements, we introduce a mathematical construct, which we will call “measurement contrast",

that characterizes the sampling complexity of DFE of a Hermitian operator $\mathcal{O}$, given a set of possible bounded measurement operators. Here, LOCC measurement refers to any measurement that involves only LOCC operations.

Definition 4. Define the traceless operator $\widetilde{\mathcal{O}}$

$$\widetilde{\mathcal{O}} = \mathcal{O} - \frac{\mathrm{tr}(\mathcal{O})}{D} I, \tag{A.8}$$

and the "effective contrast" Y

$$Y(\mathcal{O}, M, \varsigma) = \begin{cases} 0 & \textbf{if } \mathrm{tr}(M\tilde{\varsigma}) > 0, \\ \frac{\mathrm{tr}\left(M\widetilde{\mathcal{O}}\right)}{\lambda_{\max}(M) - \lambda_{\min}(M)} & \textbf{if } \mathrm{tr}(M\tilde{\varsigma}) \leq 0, \end{cases} \tag{A.9}$$

where D is the dimension of the overall Hilbert space, $\lambda_{\max}$ and $\lambda_{\min}$ are the maximum and minimum value assigned to any measurement result, and $\tilde{\varsigma} = \varsigma - \frac{I}{D}\,\mathrm{tr}(\varsigma) - \frac{\widetilde{\mathcal{O}}}{\|\widetilde{\mathcal{O}}\|_F^2}\,\mathrm{tr}\left(\varsigma\widetilde{\mathcal{O}}\right)$. Here M is a measurement operator, while ς is some Hermitian operator that will be determined later. For any Hermitian operator $\mathcal{O}$ and the set of measureable operators $\mathcal{M}$, we define the measurement contrast to be

$$Y_{\mathcal{M}}(\mathcal{O}) = \min_{\varsigma \in \mathcal{H}} \max_{M \in \mathcal{M}} Y(\mathcal{O}, M, \varsigma), \tag{A.10}$$

where $\mathcal{H}$ is the set of all Hermitian operators. If this value is positive, it implies that for any ς, there exists some $M \in \mathcal{M}$ such that $Y(\mathcal{O}, M, \varsigma) \geq Y_{\mathcal{M}}(\mathcal{O})$.

This measurement contrast, which we will demonstrate in the following theorem, indicates that there exists a random ensemble of measurements from $\mathcal{M}$ such that the expected value is proportional to the expected value of $\mathcal{O}$ with a proportional constant of at least $Y_{\mathcal{M}}(\mathcal{O})$.

Theorem 4. *Given a set of possible measurable operators $\mathcal{M}$, if $Y_{\mathcal{M}}(\mathcal{O}) > 0$, then $Z_{\mathcal{M}}(\mathcal{O}) \leq \|\widetilde{\mathcal{O}}\|_F^2 / Y_{\mathcal{M}}(\mathcal{O})$.*

Proof. In this proof, we use an iterative approach to generate an ensemble of measurements to approximate $\mathcal{O}$ with a systematic error that limits to 0 as the iteration number increases. For an ensemble of M_i and the corresponding probability distribution $p_i^{(n)}$ in the n-th iteration, we define

$$\begin{cases} \widetilde{M}_i = \dfrac{M_i - \frac{\mathrm{tr}(M_i)}{D} I}{\lambda_{\max}(M) - \lambda_{\min}(M)}, \\ \Delta_i = \widetilde{M}_i - \dfrac{\mathrm{tr}\left(\widetilde{M}_i \widetilde{\mathcal{O}}\right)}{\|\widetilde{\mathcal{O}}\|_F^2} \widetilde{\mathcal{O}} = \widetilde{M}_i - \dfrac{Y(\mathcal{O}, M_i, \varsigma_{i-1})}{\|\widetilde{\mathcal{O}}\|_F^2} \widetilde{\mathcal{O}}, \\ \varsigma_n = \sum_i p_i^{(n)} \Delta_i. \end{cases} \tag{A.11}$$

Here Δ_i is the deviation for the measurement M_i from approximating $\mathcal{O}$, while ς_n is the deviation of the ensemble at step n. We can see that Δ and ς have zero traces and zero overlaps with $\mathcal{O}$. Moreover,

$$\|\Delta_i\|_F \leq \|\widetilde{M}_i\|_F < \sqrt{D}. \tag{A.12}$$

Now we discuss how we generate the ensemble of measurement $\{M_i\}$ and the corresponding probability $p_i^{(n)}$ for each operator M_i iteratively. First, we set $\varsigma_0 = 0$. From Eq. (A.10), there exists M_1 with $\mathrm{tr}\left(\widetilde{M}_1 \widetilde{\mathcal{O}}\right) \geq Y_{\mathcal{M}}(\mathcal{O})$. We set $p_1^{(1)} = 1$ accordingly, leading to the deviation $\varsigma_1 = \Delta_1$.

Then, after finishing the n-th iteration, we will update $\{M_i\}$ and $p_i^{(n+1)}$ in the following way. Given ς_n, from Eq. (A.10), there exists M_{n+1} such that $0 \geq \mathrm{tr}(\varsigma_n M_{n+1}) = \mathrm{tr}(\varsigma_n \Delta_{n+1})$ with $\mathrm{tr}\left(\widetilde{M}_{n+1} \widetilde{\mathcal{O}}\right) \geq Y_{\mathcal{M}}(\mathcal{O})$. Set $p_{n+1}^{(n+1)} = \frac{\|\Delta_{n+1}\|_F^2}{\|\Delta_{n+1}\|_F^2 + \|\varsigma_n\|_F^2}$ and $p_i^{(n+1)} = \left(1 - p_{n+1}^{(n+1)}\right) p_i^{(n)}$, then the deviation will be $\varsigma_{n+1} = p_{n+1}^{(n+1)} \Delta_{n+1} + \left(1 - p_{n+1}^{(n+1)}\right) \varsigma_n$, which satisfies $\|\varsigma_{n+1}\|_F^{-2} \geq \|\Delta_{n+1}\|_F^{-2} + \|\varsigma_n\|_F^{-2}$. From this, we have a bound of the Frobenius norm of this new ς:

$$\|\varsigma_{n+1}\|_F \leq \left(\sum_i \|\Delta_i\|^{-2} \right)^{-1/2} < \sqrt{D/(n+1)}. \tag{A.13}$$

In the limit of n going to ∞, $\lim_{n\to\infty}\|\varsigma_n\|_F \leq \lim_{n\to\infty}\sqrt{D/n} = 0$. Therefore,

$$\lim_{n\to\infty}\left(\sum_i p_i^{(n)}\widetilde{M}_i - \sum_i p_i^{(n)}\frac{\mathrm{tr}\left(\widetilde{M}_i\widetilde{\mathcal{O}}\right)}{\|\widetilde{\mathcal{O}}\|_F^2}\widetilde{\mathcal{O}}\right) = 0. \tag{A.14}$$

Hence, we demonstrated there exists an ensemble to approximate $\mathcal{O}$:

$$Z\sum_i p_i^{(n)}\widetilde{M}_i + CI = \mathcal{O}, \tag{A.15}$$

with

$$Z = \left(\sum_i p_i^{(n)}\frac{\mathrm{tr}\left(\widetilde{M}_i\widetilde{\mathcal{O}}\right)}{\|\widetilde{\mathcal{O}}\|_F^2}\right)^{-1} \leq \frac{\|\widetilde{\mathcal{O}}\|_F^2}{Y_{\mathcal{M}}(\widetilde{\mathcal{O}})}, \tag{A.16}$$

and

$$C = \frac{\mathrm{tr}\left(\mathcal{O}\right)}{D}. \tag{A.17}$$

□

With this framework, we conjecture the following, which, when combined with Theorem 4, is a sufficient condition for DFE with only LOCC measurements to be efficient for any pure state.

Conjecture 1. *For any Hermitian operator $\mathcal{O}$ in an m-qubit system, there exists an LOCC measurement M with $\lambda_{\max} = 1$ and $\lambda_{\min} = -1$ such that*

$$\mathrm{tr}\left(M\right) = 0, \tag{A.18}$$

$$\mathrm{tr}\left(M\widetilde{\mathcal{O}}\right) \geq \left(1-2^{-m}\right)^{-1}\|\widetilde{\mathcal{O}}\|_2. \tag{A.19}$$

Corollary 10. *If Conjecture 1 holds, then for any pure state $|\psi\rangle$, $Z_{LOCC}(|\psi\rangle\langle\psi|) \leq 2 - 2^{1-m}$.*

Proof. Consider $\mathcal{O} = \widetilde{\mathcal{O}} = \left(1-2^{-m}\right)^{-1}|\psi\rangle\langle\psi| - \left(2^m-1\right)^{-1}I - \epsilon\varsigma$, where ς is a traceless

Hermitian operator satisfying $\varsigma|\psi\rangle = 0$ and ϵ is a positive number satisfying $\epsilon\|\varsigma\|_2 \leq 1 - (2^m - 1)^{-1}$, we have $\|\widetilde{\mathcal{O}}\|_2 = 1$. From conjecture 1, there exists M such that $\mathrm{tr}(M) = 0$ and

$$\begin{aligned} \mathrm{tr}\left(M\left(\widetilde{\mathcal{O}} + \epsilon\varsigma\right)\right) &= \frac{\langle\psi \,|\, M \,|\, \psi\rangle}{1 - 2^{-m}} - \frac{\mathrm{tr}\,(M)}{2^m - 1} \\ &\leq \frac{\|\widetilde{\mathcal{O}}\|_2}{1 - 2^{-m}} \leq \mathrm{tr}\left(M\widetilde{\mathcal{O}}\right). \end{aligned} \tag{A.20}$$

Hence, we have

$$\mathrm{tr}\,(M\varsigma) \leq 0. \tag{A.21}$$

$$\begin{aligned} \frac{\mathrm{tr}\left(M\left(|\psi\rangle\langle\psi| - 2^{-m}I\right)\right)}{\lambda_{\max}(M) - \lambda_{\min}(M)} &= \frac{1 - 2^{-m}}{2}\,\mathrm{tr}\left(M\left(\widetilde{\mathcal{O}} + \epsilon\varsigma\right)\right) \\ &\geq \frac{1}{2} + \frac{1 - 2^{-m}}{2}\epsilon\,\mathrm{tr}\,(M\varsigma) \\ &> \frac{1}{2}\left(1 - \epsilon\|\varsigma\|_1\right). \end{aligned} \tag{A.22}$$

Therefore, for any positive ϵ we have $Y(|\psi\rangle\langle\psi|, M, \varsigma) > \frac{1}{2}\left(1 - \epsilon\|\varsigma\|_1\right)$. Since this holds for any sufficiently small ϵ, we must have $Y_{LOCC}(|\psi\rangle\langle\psi|) \geq 1/2$. From Theorem 4, we thus have

$$Z_{LOCC}(|\psi\rangle\langle\psi|) \leq 2\||\psi\rangle\langle\psi| - 2^{-m}I\|_F^2 = 2 - 2^{1-m}. \tag{A.23}$$

□

For example, the DFE cost of any two-qubit entangled pure state with LOCC measurements is at most the same as that of a Bell pair: Any two-qubit pure state is equivalent to the Schmidt form up to single-qubit unitaries, hence without loss of generality let $|\psi\rangle = \sqrt{\lambda}|00\rangle + \sqrt{1-\lambda}|11\rangle$, with $\lambda \geq 1/2$. To perform DFE of such state with LOCC measurements, we can measure a random Pauli on a random qubit, followed by measuring the other qubit along the projected state, i.e.

$$\frac{2\hat{M}_z + \hat{M}_{x1} + \hat{M}_{x2} + \hat{M}_{y1} + \hat{M}_{y2}}{6} = \frac{2\hat{M}_\psi + I}{3}, \tag{A.24}$$

where $\hat{M}_z = |00\rangle\langle 00| + |11\rangle\langle 11|$, $\hat{M}_{x1} = |+\rangle\langle +| \otimes \left(\sqrt{\lambda}|0\rangle + \sqrt{1-\lambda}|1\rangle\right)\left(\sqrt{\lambda}\langle 0| + \sqrt{1-\lambda}\langle 1|\right) + |-\rangle\langle -| \otimes \left(\sqrt{\lambda}|0\rangle - \sqrt{1-\lambda}|1\rangle\right)\left(\sqrt{\lambda}\langle 0| - \sqrt{1-\lambda}\langle 1|\right)$, and similar for $\hat{M}_{y1}, \hat{M}_{x2}, \hat{M}_{y2}$.